

Defending Black-box Classifiers by Bayesian Boundary Correction

He Wang^{1*†} and Yunfeng Diao^{2†}

^{1*}School of Computing, University of Leeds, Woodhouse Lane, Leeds, United Kingdom.

²School of Computer Science and Information Engineering, Hefei University of Technology, Shushan District, Hefei, China.

*Corresponding author(s). E-mail(s): h.e.wang@leeds.ac.uk;

[†]These authors contributed equally to this work.

Abstract

Classifiers based on deep neural networks have been recently challenged by Adversarial Attack, where the widely existing vulnerability has invoked the research in defending them from potential threats. Given a vulnerable classifier, existing defense methods are mostly white-box and often require re-training the victim under modified loss functions/training regimes. While the model/data/training specifics of the victim are usually unavailable to the user, re-training is unappealing, if not impossible for reasons such as limited computational resources. To this end, we propose a new black-box defense framework. It can turn any pre-trained classifier into a resilient one with little knowledge of the model specifics. This is achieved by new joint Bayesian treatments on the clean data, the adversarial examples and the classifier, for maximizing their joint probability. It is further equipped with a new post-train strategy which keeps the victim intact. We name our framework Bayesian Boundary Correction (BBC). BBC is a general and flexible framework that can easily adapt to different data types. We instantiate BBC for image classification and skeleton-based human activity recognition, for both static and dynamic data. Exhaustive evaluation shows that BBC has superior robustness and can enhance robustness without severely hurting the clean accuracy, compared with existing defense methods.

Keywords: Adversarial Attack, Classification robustness, Human Activity Recognition

1 Introduction

Deep learning classifiers have been proven to be universally vulnerable to malicious perturbations on data and training, i.e. adversarial attack (AA) (Chakraborty, Alam, Dey, Chattopadhyay, & Mukhopadhyay, 2018), causing alarming concerns because such perturbations are imperceptible to humans but destructive to machine intelligence. Existing AA methods can be characterized by the amount of information required. White-box attack (Goodfellow, Shlens, & Szegedy, 2015)

assumes the access to the victim model and can compute the loss gradient with respect to samples. Transfer-based attack (Dong et al., 2018) does not require access to the victim but needs a surrogate victim. Black-box/semi black-box approaches only require access to the input/output of the victim (Brendel, Rauber, & Bethge, 2018; Ilyas, Engstrom, & Madry, 2019).

Corresponding to AA, defense methods have emerged as a new field recently (Chakraborty et

al., 2018) where most research can be categorized into data enhancement and model enhancement. Popular data enhancement methods involve finding potential adversarial examples e.g. adversarial training (AT) (Madry, Makelov, Schmidt, Tsipras, & Vladu, 2018) and randomized smoothing (RS) (Cohen, Rosenfeld, & Kolter, 2019), or removing perturbation via denoising (Nie et al., 2022). The philosophy behind them is different. The former biases the classifier by exposing it to potential threats while the latter focuses on learning an accurate representation of the data distribution. Both can be seen as robustness enhancement via adding new training samples. However, the first kind diverts the classifier towards adversarial examples, and therefore often compromises the clean accuracy (H. Zhang et al., 2019a), and the second kind largely focuses on clean data while not explicitly considering the distribution of adversarial examples and therefore is less robust (Cohen et al., 2019). In parallel, model enhancement methods explore particular architectures and training processes, e.g. adding regularization (Qin et al., 2019), using robust loss functions (Mustafa et al., 2020), employing tailored layers/activation (Xu, Li, & Li, 2022). Despite being effective in some settings, their overall performance is worse than data enhancement methods (Croce et al., 2020). Recently, Bayesian treatment on model itself has shown great promise (X. Liu, Li, Wu, & Hsieh, 2019) but is still under-explored.

Given a pre-trained vulnerable classifier, most existing defenses can be regarded as white-box approaches, i.e. requiring the full knowledge of the model and retraining the model. However, white-box defenses may not be applicable in some scenarios. From the perspective of developers, a model owner may refuse to share the model information for business or security considerations. From the perspective of end-users, large models are normally pre-trained on large datasets then shared. The end-users can directly use the pre-trained model or fine-tune it for downstream tasks. Retraining the model is computationally intensive and impractical. In addition, keeping the pre-trained model intact can also avoid undermining other tasks when the model is learned for multiple tasks. Last but not the least, unlike the pre-trained model which is trained well for benign data, robustly retraining such as AT can

severely compromise the benign accuracy for various reasons (Bai, Luo, Zhao, Wen, & Wang, 2021), which is restrictive in practice when requiring high accuracy. Therefore, it is imperative to develop a black-box defense.

In this research, we aim for a general defense framework that is compatible with any pre-trained classifier, adaptive to incorporate domain-specific inductive bias, and lightweight incurring only a small additional cost, to achieve robustness. In other words, we do not aim for the most robust defense at any cost, but a cost-effective way for gaining robustness. Our key observation is that different focus in previous approaches, i.e. denoising methods emphasizing on the data manifold, AT and RS methods targeting at the adversarial distribution, and model enhancement methods aiming for the model robustness, should be holistically considered. Therefore, we jointly model the data manifold, the adversarial distribution and the classifier, by learning the joint probability $p(\tilde{\mathbf{x}}, \mathbf{x}, \mathbf{y}, \theta)$ where \mathbf{x} and \mathbf{y} are the data and labels, $\tilde{\mathbf{x}}$ is the adversarial examples and θ is the classifier parameter. Through factorizing $p(\tilde{\mathbf{x}}, \mathbf{x}, \mathbf{y}, \theta)$, we can explicitly represent all the key distributions including the data manifold $p(\mathbf{x}, \mathbf{y})$, the adversarial distribution $p(\tilde{\mathbf{x}}|\mathbf{x}, \mathbf{y}, \theta)$ and the classifier distribution $p(\theta|\tilde{\mathbf{x}}, \mathbf{x}, \mathbf{y})$.

Specifically, we first parameterize the data distribution $p(\mathbf{x}, \mathbf{y})$ as an energy-based model (Hill, Mitchell, & Zhu, 2021; Lee, Yang, & Oh, 2020; Zhu et al., 2021). Observing that in AT different attackers can compute different adversarial examples for the same clean sample (i.e. one-to-many), we augment $p(\mathbf{x}, \mathbf{y})$ into $p(\tilde{\mathbf{x}}, \mathbf{x}, \mathbf{y})$ where a flexible adversarial distribution can be obtained $p(\tilde{\mathbf{x}}|\mathbf{x}, \mathbf{y})$ to capture the *one-to-many* mapping between the clean and the adversarial examples. Finally, although there is an infinite number of classifiers that can perfectly classify data (Neal, 2012) (i.e. accuracy equivalency), we argue they have different robustness against different adversarial examples, i.e. a specific classifier can resist the attack from some adversarial examples but not others, or robustness inequivalency. This leads to a further generalization of $p(\tilde{\mathbf{x}}, \mathbf{x}, \mathbf{y})$ into $p(\tilde{\mathbf{x}}, \mathbf{x}, \mathbf{y}, \theta)$, where the classifier posterior $p(\theta|\tilde{\mathbf{x}}, \mathbf{x}, \mathbf{y})$ considers all robust classifiers. We name our method Bayesian Boundary Correction, or BBC.

BBC is straightforward but effective. The key differences between our method and previous

Table 1 A high-level comparison between our method and existing methods. DM: data manifold. AD: adversarial distribution. CD: classifier distribution. PT: post-train

Method	DM	AD	CD	PT
AT (Madry et al., 2018)	n/a	point estimation	n/a	no
RS (Cohen et al., 2019)	n/a	simplified	n/a	no
Denoising (Nie et al., 2022)	Yes	n/a	n/a	no
Model enhancement (Xu et al., 2022)	simplified	simplified	n/a	some
Bayesian (X. Liu et al., 2019)	n/a	simplified	Yes	no
Ours	Yes	Yes	Yes	Yes

methods are shown in Tab. 1. The first novelty of BBC is that we simultaneously conduct Bayesian treatments on the data manifold, the adversarial distribution and the classifier, mainly inspired by the clean-adversarial one-to-many mapping and the robustness inequivalency of classifiers. The second novelty is we propose a new post-train defense strategy to simultaneously tackle the sampling difficulties in inference on Bayesian Neural Networks and keep the victim intact. BBC appends a small extra Bayesian component to the victim, which makes BBC applicable to pre-trained classifiers and requires minimal prior knowledge of them, achieving black-box defense.

As a result, BBC can turn pre-trained classifiers into resilient ones. It also circumvents model re-training, avoids heavy memory footprint and speeds up adversarial training. BBC leads to a general defense mechanism against a variety of attackers which are not known *a priori* during training. We evaluate BBC on a large number of classifiers on image and skeletal motion data, and compare it with existing methods. Empirically, BBC can effectively boost the robustness of classifiers against attack, and does not severely sacrifice accuracy for robustness, as opposed to the common observation of such trade-off in other methods (Yang, Rashtchian, Zhang, Salakhutdinov, & Chaudhuri, 2020).

Formally, we propose: 1) a new general and adaptive black-box defense framework. 2) a new Bayesian perspective on a joint distribution of clean data, adversarial examples and classifiers. 3) a new flexible way of incorporating domain-specific inductive biases for robust learning. 4) a new post-train Bayesian strategy to keep the blackboxness of classifiers and avoid heavy memory footprint.

Our paper is an extension of (H. Wang, Diao, Tan, & Guo, 2023). In this journal extension, we have extended the previous work to image classification tasks with new evaluation and comparison, added more details of the derivation of the model and the inference method, included a wider and deeper literature review and conducted more analysis and discussion.

2 Related Work

Adversarial Attack.

Since identifying the vulnerability in deep learning models for the first time (Goodfellow et al., 2015), the community has developed numerous adversarial attacks (Chakraborty et al., 2018). Many of these attacks involve computing or estimating the gradient of the model to generate adversarial examples under both the white-box and black-box settings (P.-Y. Chen, Zhang, Sharma, Yi, & Hsieh, 2017; Goodfellow et al., 2015; Ilyas et al., 2019; Kurakin, Goodfellow, & Bengio, 2016; Madry et al., 2018). Later, the discovery of the gradient obfuscation phenomenon prompts the development of adaptive attacks (Athalye, Carlini, & Wagner, 2018; Tramer, Carlini, Brendel, & Madry, 2020). While static data has attracted most of the attention, the attack on time-series data has recently emerged *e.g.* in general time-series analysis (Karim, Majumdar, & Darabi, 2020) and video classification (Pony, Naeh, and Mannor (2021); X. Wei, Zhu, Yuan, and Su (2019); Z. Wei et al. (2020)). Unlike static data, time-series data contains rich dynamics, which makes it difficult to adapt generic methods (Brendel et al., 2018; Madry et al., 2018). Therefore, time-series attacks need to be carefully designed for specific data types (H. Wang, He, et al., 2021). Very recently,

skeleton-based Human Activity Recognition (S-HAR) classifiers, one active sub-field in dynamic data, has been shown to be extremely vulnerable (Diao, Shao, Yang, Zhou, & Wang, 2021; J. Liu, Akhtar, & Mian, 2020; Tanaka, Kera, & Kawamoto, 2021; H. Wang, He, et al., 2021), calling for mitigation.

Adversarial Training (AT).

AT methods (Bai et al., 2021; Goodfellow et al., 2015) are among the most effective defense techniques to date. Recently, different training strategies are designed to significantly improve the vanilla AT (Madry et al., 2018). Wang et al. (Y. Wang et al., 2020) examine the impact of misclassified examples on AT, and introduce a regularization technique that explicitly distinguishes misclassified examples (MART). AWP (Wu, Xia, & Wang, 2020) enhances robustness by regularizing the flatness of the weight loss landscape. LAS-AT (Jia et al., 2022) explores a dynamic adversary sampling in AT. While effective in improving robustness, AT forces the classifier to correctly classify the most aggressive adversarial example during training at the cost of clean accuracy (Madry et al., 2018; Y. Wang et al., 2020; H. Zhang et al., 2019b), which is regarded as an inherent trade-off between clean accuracy and adversarial robustness (Tsipras, Santurkar, Engstrom, Turner, & Madry, 2019; Yang et al., 2020). TRADES (H. Zhang et al., 2019b) controls the trade-off between accuracy and robustness by constraining the difference in output probabilities between clean samples and their adversarial counterparts. More recent attempts to alleviate the accuracy-robustness trade-off include early-stopping version of AT (Rice, Wong, & Kolter, 2020; J. Zhang et al., 2020), studying the manifold of adversaries and clean data (Diao et al., 2022; Stutz, Hein, & Schiele, 2019), using natural classifier boundary guidance (Cui, Liu, Wang, & Jia, 2021), and reducing excessive margin along adversarial directions (Rade & Moosavi-Dezfooli, 2022). Despite these advancements, this problem remains far from being solved, as there still exists an obvious gap between accuracy and robustness. Infinite data assumption (Raghunathan, Xie, Yang, Duchi, & Liang, 2020) theoretically can eliminate the trade-off. Gowal, Qin, Uesato, Mann, and

Kohli (2020) also suggest that the robust generalization can be remarkably improved by largely using extra data in AT. We revisit this issue in our paper and narrow the gap even further, without requiring extra data and retraining the model.

So far, most AT studies have focused on static data, e.g. image data, leaving defense for time-series domain less explored. Very recently, AT for video classification (Kinfu & Vidal, 2022), finance (Z. Zhang et al., 2023) and S-HAR (Diao et al., 2022) have just been attempted. However, they are all designed for specific data and tasks, and hence difficult to be adaptive to other data types. In this paper, we further propose a general defense framework that can adapt to different data types by incorporating domain-specific inductive biases for robust learning.

Bayesian Defense.

Bayesian Neural Networks (BNNs) (Neal, 2012) with the capabilities of modeling uncertainty have shown great promise in defending against adversarial examples. Carbone et al. (2020) theoretically demonstrate that BNNs are robust to gradient-based adversarial attacks in the over-parameterization and large data limit. Ye and Zhu (2018) propose Bayesian adversarial learning to incorporate the uncertainty of data and model parameters. X. Liu et al. (2019) scale Bayesian adversarial training to more complex data and add randomness to all weights in the network. Further, Doan, Abbasnejad, Shi, and Ranasinghe (2022) employ Stein Variational Gradient Descent (Q. Liu & Wang, 2016) for better sampling the posterior distribution, and to maintain the same measure of information content learned from the given input and its adversarial counterpart. Although combining BNNs with adversarial training has been recently suggested as a robust deep learning paradigm, training BNNs is a significant challenge since sampling the posterior distribution is intractable in the high-dimensional space of deep neural networks (Blei, Kucukelbir, & McAuliffe, 2017). To mitigate this issue, we propose a post-train Bayesian strategy which enables a black-box defense and fast training.

Black-box Defense.

Black-box or post-processing defense has been largely unexplored, despite (S. Chen et al., 2022;

H. Wang et al., 2023; Y. Zhang et al., 2022). Y. Zhang et al. (2022) study the certified black-box defense from a zeroth-order optimization perspective. S. Chen et al. (2022) propose to perturb the DNN’s output scores to fool the attackers, but such a defense strategy is only effective for preventing score-based query attacks and is not applicable to other types of attacks such as gradient-based attacks. H. Wang et al. (2023) propose the first black-box defense for S-HAR. In this paper, we propose a new general black-box defense framework, adaptive to different data types. We empirically demonstrate that BBC can defend both white-box and black-box attacks without sacrificing accuracy.

3 Methodology

We first introduce the background of energy-based models in Sec. 3.1. Then we introduce our Bayesian treatment on the adversarial samples under the energy-based modeling in Sec. 3.2. In Sec. 3.3, we further introduce our Bayesian classifier and the post-train Bayesian strategy. In Sec. 3.4, we explain the inference method. Finally, we instantiate our proposed method for both static and dynamic data in Sec. 3.5.

3.1 Energy-based Models

Given data $\mathbf{x} \in \mathbf{X}$ and label \mathbf{y} , a discriminative classifier can be generalized from an energy perspective by modeling the joint distribution $p_\theta(\mathbf{x}, y) = \frac{\exp(g_\theta(\mathbf{x})[y])}{Z(\theta)}$ where $y \in \mathbf{y}$ and θ is the model parameters (Grathwohl et al., 2020). Since $p_\theta(\mathbf{x}, y) = p_\theta(y|\mathbf{x})p_\theta(\mathbf{x})$ and $p_\theta(y|\mathbf{x})$ is what classifiers maximize, the key difference is $p_\theta(\mathbf{x})$ which can be parameterized by an energy function:

$$p_\theta(\mathbf{x}) = \frac{\exp(-E_\theta(\mathbf{x}))}{Z(\theta)} = \frac{\sum_{y \in \mathbf{y}} \exp(g_\theta(\mathbf{x})[y])}{Z(\theta)} \quad (1)$$

where E_θ is an energy function parameterized by θ , $Z(\theta) = \int_{\mathbf{x}} \exp(-E_\theta(\mathbf{x})) d\mathbf{x}$ is a normalizing constant. This energy-based interpretation allows an arbitrary E_θ to describe a continuous density function, as long as it assigns low energy values to observations and high energy everywhere else. This leads to a generalization of discriminative classifiers: E can be an exponential function

as shown in Eq. (1) where g_θ is a classifier and $g_\theta(\mathbf{x})[y]$ gives the y th logit for class y . θ can be learned via maximizing the log likelihood:

$$\log p_\theta(\mathbf{x}, y) = \log p_\theta(y|\mathbf{x}) + \log p_\theta(\mathbf{x}) \text{ where} \\ p_\theta(y|\mathbf{x}) = \frac{p_\theta(\mathbf{x}, y)}{p_\theta(\mathbf{x})} = \frac{\exp(g_\theta(\mathbf{x})[y])}{\sum_{y' \in \mathbf{y}} \exp(g_\theta(\mathbf{x})[y'])} \quad (2)$$

Compared with only maximizing $\log p(y|\mathbf{x})$ as discriminative classifiers do, maximizing $\log p(\mathbf{x}, y)$ can provide many benefits such as good accuracy, robustness and out-of-distribution detection (Grathwohl et al., 2020).

3.2 Joint Distribution of Data and Adversaries

A robust classifier that can resist adversarial attacks, i.e. correctly classifying both the clean \mathbf{x} and the adversarial samples $\tilde{\mathbf{x}}$, needs to consider the clean data, the adversarial samples and the attacker simultaneously:

$$g_\theta(\mathbf{x}) = g_\theta(\tilde{\mathbf{x}}) \text{ where } \tilde{\mathbf{x}} = \mathbf{x} + \sigma, \sigma \in \pi \quad (3)$$

where a classifier g_θ takes an input and outputs a class label, and σ is drawn from some perturbation set π , computed by an attacker. Since the attacker is not known *a priori*, g_θ needs to capture the whole adversarial distribution to be able to resist potential attacks post-train.

However, modeling the adversarial distribution is non-trivial as they are not observed during training. This has led to two strategies: defending against the most adversarial sample from an attacker (a.k.a Adversarial Training or AT (Madry et al., 2018)) or training on data with noises (a.k.a Randomized Smoothing or RS (Lecuyer, Atlidakis, Geambasu, Hsu, & Jana, 2019)). However, both approaches lead to a trade-off between accuracy and robustness (Yang et al., 2020). We speculate that it is because neither can fully capture the adversarial distribution.

We start from a straightforward yet key conceptual deviation from literature (Chakraborty et al., 2018): assuming there is an adversarial distribution over all adversarial examples which could be computed by all possible attackers. This assumption is driven by the observation that different attackers in AT might compute different adversarial examples even for the same clean

example, indicating that there is a distribution of adversarial examples given one clean example. Further, although it is hard to depict the adversarial distribution directly, all adversarial examples are close to the clean data (Diao et al., 2021). So for a vulnerable classifier, they also have relatively low energy. Therefore, we add the adversarial samples $\tilde{\mathbf{x}}$ to the joint distribution $p(\mathbf{x}, \tilde{\mathbf{x}}, y)$, and further extend it into a new clean-adversarial energy-based model:

$$p_{\theta}(\mathbf{x}, \tilde{\mathbf{x}}, y) = \frac{\exp\{g_{\theta}(\mathbf{x})[y] + g_{\theta}(\tilde{\mathbf{x}})[y] - \lambda d(\mathbf{x}, \tilde{\mathbf{x}})\}}{Z(\theta)} \quad (4)$$

where \mathbf{x} and $\tilde{\mathbf{x}}$ are the clean examples and their corresponding adversaries under class y . λ is a weight and $d(\mathbf{x}, \tilde{\mathbf{x}})$ measures the distance between the clean samples and their adversaries. Eq. (4) bears two assumptions. First, adversaries are in the low-energy (high-density) area as they are very similar to data. Also, their energy should increase (or density should decrease) when they deviate away from the clean samples, governed by $d(\mathbf{x}, \tilde{\mathbf{x}})$.

Further, $p_{\theta}(\mathbf{x}, \tilde{\mathbf{x}}, y)$ can be factorized as:

$$p_{\theta}(\mathbf{x}, \tilde{\mathbf{x}}, y) = p_{\theta}(\tilde{\mathbf{x}}|\mathbf{x}, y)p_{\theta}(\mathbf{x}, y) \quad (5)$$

where $p_{\theta}(\mathbf{x}, y)$ is the same as in Eq. (2). $p_{\theta}(\tilde{\mathbf{x}}|\mathbf{x}, y)$ is a new term. To further understand this term, for each data sample \mathbf{x} , we take a Bayesian perspective and assume there is a distribution of adversarial samples $\tilde{\mathbf{x}}$ around \mathbf{x} . This assumption is reasonable as every adversarial sample can be traced back to a clean sample (*i.e.* every adversarial example should be visually similar to some clean example), and there is a *one-to-many* mapping from the clean samples to the adversarial samples. Then $p_{\theta}(\tilde{\mathbf{x}}|\mathbf{x}, y)$ is a *full Bayesian treatment* of all adversarial samples:

$$p_{\theta}(\tilde{\mathbf{x}}|\mathbf{x}, y) = \frac{p_{\theta}(\mathbf{x}, \tilde{\mathbf{x}}, y)}{p_{\theta}(\mathbf{x}, y)} = \exp\{g_{\theta}(\tilde{\mathbf{x}})[y] - \lambda d(\mathbf{x}, \tilde{\mathbf{x}})\} \quad (6)$$

where the intractable $Z(\theta)$ is conveniently cancelled. Eq. (6) is a key component in BBC as it provides an energy-based parameterization, so that we are sure adversarial samples will be given low energy values and thus high density (albeit unnormalized). Through Eq. (6), our classifier is now capable of taking the adversarial sample distribution into consideration during training.

3.2.1 Connections to Existing Defense Methods

BBC has intrinsic connections with Adversarial Training (AT) and Randomised smoothing (RS). Since the potential attacker is unknown *a priori*, $d(\mathbf{x}, \tilde{\mathbf{x}})$ in Eq. 4 needs to capture the full adversarial distribution. In this sense, properly instantiating $d(\mathbf{x}, \tilde{\mathbf{x}})$ can recover both AT and RS.

AT optimizes (Madry et al., 2018):

$$\min_{\theta} E_{\mathbf{x}}[\max_{\sigma \in S} L(\theta, \mathbf{x} + \sigma, y)] \quad (7)$$

where L is the classification loss function, σ is a perturbation from a set S which is normally constrained within a ball and σ needs to be computed by a pre-defined attacker. Here, a basic AT is recovered when $d(\mathbf{x}, \tilde{\mathbf{x}})$ is the Euclidean distance between \mathbf{x} and $\tilde{\mathbf{x}}$ within the ball S .

In RS, the robust classifier is obtained through (Cohen et al., 2019):

$$\arg \max_{y \in \mathcal{Y}} p(g_{\theta}(\mathbf{x} + \sigma) = y) \text{ where } \sigma \sim \mathbf{N} \quad (8)$$

where a perturbation σ is drawn from an isotropic Gaussian. $d(\mathbf{x}, \tilde{\mathbf{x}})$ essentially plays the role of the Gaussian to describe the perturbation.

However, neither AT nor RS can capture the fine-grained structure of the adversarial distribution, because AT merely uses the most aggressive adversarial example, and RS often employs simple *isotropic* distributions (*e.g.* Gaussian/Laplacian) (D. Zhang, Ye, Gong, Zhu, & Liu, 2020). Therefore, we argue $d(\mathbf{x}, \tilde{\mathbf{x}})$ should be data/task specific and should not be restricted to isotropic forms. This is because adversarial samples are near the data manifold, both on-manifold and off-manifold (Diao et al., 2021), so the data manifold geometry should dictate the parameterization of $d(\mathbf{x}, \tilde{\mathbf{x}})$. A proper $d(\mathbf{x}, \tilde{\mathbf{x}})$ allows us to sample in the space that is expanded from the manifold in a potentially non-isotropic way, like adding a ‘thickness’ to the data manifold.

In general, there are two possible avenues to model the data manifold: implicit and explicit. Explicit formulations can be used if it is relatively straightforward to parameterize the manifold geometry; or a data-driven model can be used to implicitly learn the manifold. Either way,

the manifold can then be devised with a distance function to instantiate $d(\mathbf{x}, \tilde{\mathbf{x}})$.

3.3 Bayesian Classifier for Further Robustness

Although Eq. (4) considers the full distribution of the data and the adversarial examples, it is still a *point estimation* with respect to the model θ . From a Bayesian perspective, there is a distribution of models which can correctly classify \mathbf{x} , *i.e.* there is an infinite number of ways to draw the classification boundaries (accuracy equivalency). Our insight is these models can vary in terms of their robustness (robustness inequivalency). Intuitively, a single boundary can be robust against certain adversaries, *e.g.* the distance between the boundary and some clean data examples are large hence requiring larger perturbations for attack. However, they might not be similarly robust against other adversaries. A collection of all boundaries can be more robust because they provide different between-class distances (Yang et al., 2020) and local boundary continuity (C. Liu, Salzmänn, Lin, Tomioka, & Süssstrunk, 2020), which are all good sources for robustness. Therefore, we augment Eq. (4) to incorporate the network weights θ :

$$p(\theta, \mathbf{x}, \tilde{\mathbf{x}}, y) = p(\mathbf{x}, \tilde{\mathbf{x}}, y | \theta) p(\theta) \quad (9)$$

where $p(\mathbf{x}, \tilde{\mathbf{x}}, y | \theta)$ is essentially Eq. (4) and $p(\theta)$ is the prior of network weights. This way, we have a new Bayesian joint model of clean data, adversarial examples and the classifier. From the Bayesian perspective, maximizing Eq. (4) is equivalent to using a flat $p(\theta)$ and applying iterative *Maximum a posteriori* (MAP) optimization. However, even with a flat prior, a MAP optimization is still a point estimation on the model, and cannot fully utilize the full posterior distribution (Saatci & Wilson, 2017). In contrast, we propose to use *Bayesian Model Averaging*:

$$\begin{aligned} p(y' | \mathbf{x}', \mathbf{x}, \tilde{\mathbf{x}}, y) &= E_{\theta \sim p(\theta)} [p(y' | \mathbf{x}', \mathbf{x}, \tilde{\mathbf{x}}, y, \theta)] \\ &\approx \frac{1}{N} \sum_{i=1}^N p(y' | \mathbf{x}', \theta_i), \theta \sim p(\theta | \mathbf{x}, \tilde{\mathbf{x}}, y) \end{aligned} \quad (10)$$

where \mathbf{x}' and y' are a new sample and its predicted label, $p(\theta)$ is a flat prior, N is the number of models. We expect such a Bayesian classifier to be

more robust against attack while achieving good accuracy, because models from the high probability regions of $p(\theta | \mathbf{x}, \tilde{\mathbf{x}}, y)$ provide both. This is vital as we do not know the attacker in advance. To train such a classifier, the posterior distribution $p(\theta | \mathbf{x}, \tilde{\mathbf{x}}, y)$ needs to be sampled as it is intractable.

3.3.1 Necessity of a Post-train Bayesian Strategy

Unfortunately, it is not straightforward to design such a Bayesian treatment (Eq. (10)) on pre-trained classifiers due to several factors. First, sampling the posterior distribution $p(\theta | \mathbf{x}, \tilde{\mathbf{x}}, y)$ is prohibitively slow. Considering the large number of parameters in classifiers (possibly over several million), sampling would mix extremely slowly in such a high dimensional space (if at all).

In addition, from the perspective of end-users, large models are normally pre-trained on large datasets then shared. The end-users can fine-tune or directly use the pre-trained model. It is not desirable/possible to re-train the models. This can be because the owner of the model refuses to share the model details and only provide APIs for access, or they cannot share the training data for security/ethical reasons, or simply the end-users do not have necessary computing capacity to retrain the model.

Finally, most classifiers consist of two parts: feature extraction and boundary computation. The data is pulled through the first part to be mapped into a latent feature space, then the boundary is computed, *e.g.* through fully-connected layers. The feature extraction component is well learned in the pre-trained model. Keeping the features intact can avoid re-training the model, and avoid undermining other tasks when the features are learned for multiple tasks, *e.g.* under representation/self-supervised learning.

Therefore, we propose a *post-train* Bayesian strategy for black-box defense. We keep the pre-trained classifier intact and append a tiny model with parameters θ' behind the classifier using a skip connection: $g_{\theta'}(\mathbf{x}) = f_{\theta'}(\phi(\mathbf{x})) + g_{\theta}(\mathbf{x})$, in contrast to the original logits $= g_{\theta}(\mathbf{x})$. $\phi(\mathbf{x})$ can be the latent features of \mathbf{x} or the original logits $\phi(\mathbf{x}) = g_{\theta}(\mathbf{x})$. We employ the latter setting based on the ablation studies in Sec. 4.4 and to keep the *blackboxness* of BBC. We can replace all the $g_{\theta}(\mathbf{x})$ above with $g_{\theta'}(\mathbf{x})$ now.

The appended model $f_{\theta'}$ can be an arbitrary network. Eq. (10) then becomes:

$$\begin{aligned} p(y'|\mathbf{x}', \mathbf{x}, \tilde{\mathbf{x}}, y) &= E_{\theta' \sim p(\theta')} [p(y'|\mathbf{x}', \mathbf{x}, \tilde{\mathbf{x}}, y, \theta, \theta')] \\ &\approx \frac{1}{N} \sum_{i=1}^N p(y'|\mathbf{x}', \theta'_i, \theta), \theta' \sim p(\theta'|\mathbf{x}, \tilde{\mathbf{x}}, y, \theta) \end{aligned} \quad (11)$$

where θ is fixed after pre-training and we do not change it. Then BBC training can be conducted through alternative sampling:

$$\begin{aligned} \{\mathbf{x}, \tilde{\mathbf{x}}, y\}_t | \theta, \theta'_{t-1} &\sim p(\mathbf{x}, \tilde{\mathbf{x}}, y | \theta, \theta'_{t-1}) \\ \theta'_t | \{\mathbf{x}, \tilde{\mathbf{x}}, y\}_t, \theta &\sim p(\theta' | \{\mathbf{x}, \tilde{\mathbf{x}}, y\}_t, \theta) \end{aligned} \quad (12)$$

Although $f_{\theta'}$ can be any model, surprisingly a simple two-layer fully-connected layer network (with the same dimension as the original output) proves to work well in all cases. During attack, we attack the full model $g_{\theta'}$. We use $N = 5$ models in all experiments and explain the reason in the ablation study later. Overall, since $f_{\theta'}$ is much smaller than g_{θ} , training $g_{\theta'}$ is faster than re-training g_{θ} .

3.4 Inference on BBC

Following Eq. (12), in each iteration, we sample θ' by Stochastic Gradient Hamiltonian Monte Carlo (T. Chen, Fox, & Guestrin, 2014). However, we find that it cannot efficiently explore the target density due to the high correlations between parameters in θ' . Therefore, we use Stochastic Gradient Adaptive Hamiltonian Monte Carlo (Springenberg, Klein, Falkner, & Hutter, 2016):

$$\begin{aligned} \theta'_{t+1} &= \theta'_t - \sigma^2 \mathbf{C}_{\theta'_t}^{-1/2} \mathbf{h}_{\theta'_t} + \mathbf{N}(0, 2F\sigma^3 \mathbf{C}_{\theta'_t}^{-1} - \sigma^4 \mathbf{I}) \\ \mathbf{C}_{\theta'_t} &\leftarrow (1 - \tau^{-1}) \mathbf{C}_{\theta'_t} + \tau^{-1} \mathbf{h}_{\theta'_t}^2 \end{aligned} \quad (13)$$

where σ is the step size, F is called friction coefficient, \mathbf{h} is the stochastic gradient of the system, \mathbf{N} is a Normal distribution and \mathbf{I} is an identity matrix, \mathbf{C} is a pre-conditioner and updated by an exponential moving average and τ is chosen automatically (Springenberg et al., 2016).

With all the other factors fixed and starting from some initial θ'_0 , iteratively using Eq. (13) will

lead to different θ'_{t+1} s that are all samples from the posterior $p(\theta' | \{\mathbf{x}, \tilde{\mathbf{x}}, y\}_t, \theta)$. The key component in Eq. (13) is the gradient of the system \mathbf{h} . For BBC, the natural option is to follow the gradient that maximizes the log-likelihood of the joint probability (Eq. (4)):

$$\begin{aligned} \log p_{\theta'}(\mathbf{x}, \tilde{\mathbf{x}}, y) &= \log p_{\theta'}(\tilde{\mathbf{x}}|\mathbf{x}, y) + \log p_{\theta'}(\mathbf{x}, y) \\ &= \log p_{\theta'}(\tilde{\mathbf{x}}|\mathbf{x}, y) + \log p_{\theta'}(y|\mathbf{x}) + \log p_{\theta'}(\mathbf{x}) \end{aligned} \quad (14)$$

where y is randomly sampled and $\log p_{\theta'}(y|\mathbf{x})$ is simply a classification likelihood and can be estimated via *e.g.* cross-entropy. Both $p_{\theta'}(\mathbf{x})$ and $p_{\theta'}(\tilde{\mathbf{x}}|\mathbf{x}, y)$ are intractable, so sampling is needed.

To computer \mathbf{h} from Equation (14), we need to compute three gradients $\frac{\partial \log p_{\theta'}(\tilde{\mathbf{x}}|\mathbf{x}, y)}{\partial \theta'}$, $\frac{\partial \log p_{\theta'}(y|\mathbf{x})}{\partial \theta'}$ and $\frac{\partial \log p_{\theta'}(\mathbf{x})}{\partial \theta'}$. Instead of directly maximizing $\log p_{\theta'}(y|\mathbf{x})$, we minimize the *cross-entropy* on the logits, so $\frac{\partial \log p_{\theta'}(y|\mathbf{x})}{\partial \theta'}$ is straightforward. Next, $\frac{\partial \log p_{\theta'}(\mathbf{x})}{\partial \theta'}$ can be approximated by (Nijkamp, Hill, Han, Zhu, & Wu, 2019):

$$\begin{aligned} \frac{\partial \log p_{\theta'}(\mathbf{x})}{\partial \theta'} &\approx \frac{\partial}{\partial \theta'} \left[\frac{1}{L_1} \sum_{i=1}^{L_1} U(g_{\theta'}(\mathbf{x}_i^+)) \right. \\ &\quad \left. - \frac{1}{L_2} \sum_{i=1}^{L_2} U(g_{\theta'}(\mathbf{x}_i^-)) \right] \end{aligned} \quad (15)$$

where U gives the mean over the logits, $\{\mathbf{x}_i^+\}_{i=1}^{L_1}$ are a batch of training samples and $\{\mathbf{x}_i^-\}_{i=1}^{L_2}$ are i.i.d. samples from $p_{\theta'}(\mathbf{x})$ via Stochastic Gradient Langevin Dynamics (SGLD) (Welling & Teh, 2011):

$$\begin{aligned} \mathbf{x}_{t+1}^- &= \mathbf{x}_t^- + \frac{\epsilon^2}{2} \frac{\partial \log p_{\theta'}(\mathbf{x}_t^-)}{\partial \mathbf{x}_t^-} + \epsilon E_t, \epsilon > 0, \\ E_t &\in \mathbf{N}(0, \mathbf{I}) \end{aligned} \quad (16)$$

where ϵ is a step size, \mathbf{N} is a Normal distribution and \mathbf{I} is an identity matrix.

Similarly for $\frac{\partial \log p_{\theta'}(\tilde{\mathbf{x}}|\mathbf{x}, y)}{\partial \theta'}$:

$$\frac{\partial \log p_{\theta'}(\tilde{\mathbf{x}}|\mathbf{x}, y)}{\partial \theta'} = \frac{\partial}{\partial \theta'} \{g_{\theta'}(\tilde{\mathbf{x}})[y] - \lambda d(\mathbf{x}, \tilde{\mathbf{x}})\} \quad (17)$$

where $\tilde{\mathbf{x}}$ can be sampled via:

$$\tilde{\mathbf{x}}_{t+1} = \tilde{\mathbf{x}}_t + \frac{\epsilon^2}{2} \frac{\partial \log p_{\theta'}(\tilde{\mathbf{x}}_t | \mathbf{x}, y)}{\partial \tilde{\mathbf{x}}_t} + \epsilon E_t, \quad (18)$$

$$\epsilon > 0, E_t \in \mathbf{N}(0, \mathbf{I}) \quad (19)$$

Further, instead of naive SGLD, we use Persistent Contrastive Divergence (Tieleman, 2008) with a random start (Du & Mordatch, 2020). The BBC inference is detailed in Algorithm 1.

3.5 Instantiating BBC for Different Data and Tasks

So far, BBC has been introduced in a general setting. In this paper, we instantiate BBC for two types of widely investigated data: image data in image classification and skeleton motion data in S-HAR. The former is a general classification task which has been heavily studied, while the latter is time-series data which contains rich dynamics. Given the flexible setting of BBC, the instantiating is through specifying $d(\mathbf{x}, \tilde{\mathbf{x}})$ in Equation (6), where we introduce domain-specific inductive biases. Our general idea is that $d(\mathbf{x}, \tilde{\mathbf{x}})$ should faithfully reflect the distance of any sample from the underlying data manifold, as discussed in Sec. 3.2.1.

3.5.1 Perceptual Distance for BBC in Images Classification

A key assumption of BBC is all adversarial samples are imperceptible to humans and hence are distributed closely to the data manifold. This assumption relies on the data manifold being highly tuned with human visual perception, such that the data manifold can be accurately described by the true perceptual distance (Laidlaw, Singla, & Feizi, 2021). However, the true perceptual distance cannot be directly computed for image data. Considering that the perceptual similarity can be intuitively linked to the deep visual representation (R. Zhang, Isola, Efros, Shechtman, & Wang, 2018), we propose to use neural perceptual distance, i.e. a neural network-based approximation of the true perceptual distance.

The neural perceptual distance LPIPS (R. Zhang et al., 2018) has been suggested as a good surrogate for human vision, hence we define $d(\mathbf{x}, \tilde{\mathbf{x}})$ via LPIPS. LPIPS needs to learn

Algorithm 1: Inference on BBC

```

1 Input:  $\mathbf{x}$ : training data;  $N_{tra}$ : the number
  of training iterations;  $M_1$  and  $M_2$ :
  sampling iterations;  $M_{\theta'}$ : sampling
  iterations for  $\theta'$ ;  $f_{\theta'}$ : appended models
  with parameter  $\{\theta'_1, \dots, \theta'_N\}$ ;  $N$ : the
  number of appended models;
2 Output:  $\{\theta'_1, \dots, \theta'_N\}$ : appended network
  weights;
3 Init: randomly initialize  $\{\theta'_1, \dots, \theta'_N\}$ ;
4 for  $i = 1$  to  $N_{tra}$  do
5   for  $n = 1$  to  $N$  do
6     Randomly sample a mini-batch
       data  $\{\mathbf{x}, y\}_i$ ;
7     Compute  $h_1 = \frac{\partial \log p_{\theta'}(y | \mathbf{x})}{\partial \theta'}$ ;
8     Obtain  $\mathbf{x}_0$  via random noise (Du &
       Mordatch, 2020);
9     for  $t = 1$  to  $M_1$  do
10      Sample  $\mathbf{x}_t$  from  $\mathbf{x}_{t-1}$  via
        Eq. (16);
11    end
12    Compute  $h_2 = \frac{\partial \log p_{\theta'}(\mathbf{x})}{\partial \theta'}$  via
       Eq. (15);
13    Obtain  $\tilde{\mathbf{x}}_0$  from  $\mathbf{x}_i$  with a
       perturbation;
14    for  $t = 1$  to  $M_2$  do
15      Sample  $\tilde{\mathbf{x}}_t$  from  $\tilde{\mathbf{x}}_{t-1}$  via
        Eq. (18);
16    end
17    Compute  $h_3 = \frac{\partial \log p_{\theta'}(\tilde{\mathbf{x}} | \mathbf{x}, y)}{\partial \theta'}$  via
       Eq. (17);
18     $\mathbf{h}_{\theta'} = h_1 + h_2 + h_3$ ;
19    for  $t = 1$  to  $M_{\theta'}$  do
20      Update  $\theta'_n$  with  $\mathbf{h}_{\theta'}$  via Eq. (13);
21    end
22  end
23 end
24 return  $\{\theta'_1, \dots, \theta'_N\}$ ;

```

a network $h(\cdot)$ to compute the feature distances. We first extract a feature stack from L layers in $h(\cdot)$ and normalize them across the channel dimension. Let $\hat{h}_l(\mathbf{x})$ denote the internal channel-normalized activation at the l -th layer. Finally, $\hat{h}_l(\mathbf{x})$ is normalized again by the layer size and the perception distance $d(\mathbf{x}, \tilde{\mathbf{x}})$ is defined as:

$$d(\mathbf{x}, \tilde{\mathbf{x}}) = \sum_l^L w_l \left\| \frac{\hat{h}_l(\mathbf{x})}{\sqrt{W_l H_l}} - \frac{\hat{h}_l(\tilde{\mathbf{x}})}{\sqrt{W_l H_l}} \right\|_2^2 \quad (20)$$

where W_l and the H_l are the width and height of the activations in layers l , w_l is the weights. This distance function helps to quantify the perceptual similarity between a clean sample and its adversarial counterpart \mathbf{x} , so Eq. (20) describes the adversarial distribution near the image manifold. In theory, any good representation learner can be used as $h(\cdot)$. In practice, we find using a pre-trained AlexNet network can achieve a good robust performance, so we employ it as $h(\cdot)$ in image experiments.

3.5.2 Natural Motion Manifold for BBC in S-HAR

The motion manifold is well described by the motion dynamics and bone lengths (Tang et al., 2022; H. Wang, Ho, & Komura, 2015; H. Wang, Ho, Shum, & Zhu, 2021; H. Wang, Sidorov, Sandilands, & Komura, 2013). Therefore, we design d so that the energy function in Eq. (6) also assigns low energy values to the adversarial samples bearing similar motion dynamics and bone lengths:

$$d(\mathbf{x}, \tilde{\mathbf{x}}) = \frac{1}{MB} \sum \|BL(\mathbf{x}) - BL(\tilde{\mathbf{x}})\|_p^2 + \frac{1}{MJ} \sum \|q_{m,j}^k(\mathbf{x}) - \tilde{q}_{m,j}^k(\tilde{\mathbf{x}})\|_p^2 \quad (21)$$

where $\mathbf{x}, \tilde{\mathbf{x}} \in \mathbb{R}^{M \times 3J}$ are motions containing a sequence of M poses (frames), each of which contains J joint locations and B bones. BL computes the bone lengths in each frame. $q_{m,j}^k$ and $\tilde{q}_{m,j}^k$ are the k th-order derivative of the j th joint in the m th frame in the clean sample and its adversarial respectively. $k \in [0, 2]$. This is because a dynamical system can be represented by a collection of derivatives at different orders. For human motions, we empirically consider the first three orders: position, velocity and acceleration. High-order information can also be considered but would incur extra computation. $\|\cdot\|_p$ is the ℓ_p norm. We set $p = 2$ but other values are also possible. Overall, the first term is a bone-length energy and the second one is motion dynamics energy. Both energy terms together define a distance function centered at a clean data \mathbf{x} . This distance

function helps to quantify how likely an adversarial sample near \mathbf{x} is, so Eq. (21) describes the adversarial distribution near the motion manifold.

4 Experiments

4.1 Experiments on Image Classification

4.1.1 Experimental Settings

To verify BBC on image data, we employ three popular image datasets, i.e. CIFAR-10 (Krizhevsky, Hinton, et al., 2009), CIFAR-100 (Krizhevsky et al., 2009) and STL-10 (Coates, Ng, & Lee, 2011). Since our work is closely related to the Bayesian defense strategy, we choose state-of-the-art Bayesian defense methods Adv-BNN (X. Liu et al., 2019) and IG-BNN (Doan et al., 2022) as baselines. To ensure a fair comparison with other Bayesian defense methods, we adopted their default settings (Doan et al., 2022; X. Liu et al., 2019; Ye & Zhu, 2018). Specially, we use the VGG-16 network on CIFAR-10 as the target network. On STL-10, we use the smaller ModelA network used in Adv-BNN (X. Liu et al., 2019) and IG-BNN (Doan et al., 2022). Unlike existing Bayesian defense methods which are only feasible on small networks (Doan et al., 2022; X. Liu et al., 2019), BBC can also be used on larger networks such as WideResNets (Zagoruyko & Komodakis, 2016) since our proposed *post-train* Bayesian strategy can avoid heavy memory footprint. To demonstrate its effectiveness, We compare the results on WideResNets with state-of-the-art AT methods, which are the most commonly used defense strategies. We note that most AT works on CIFAR-10 and CIFAR-100 use either a WRN28-10 or a WRN34-10 network, we choose WRN28-10 on CIFAR-10 and WRN34-10 on CIFAR-100. Finally, for empirical black-box defense, there is no method for direct comparison except for AAA (S. Chen et al., 2022), so we choose it as another baseline. The training details of BBC are reported in Appendix B.

Attack Setting.

The defenses are assessed by several gradient-based attacks under the l_∞ and l_2 setting. White-box attacks includes vanilla PGD (Madry et al., 2018), EoT-PGD (Athalye, Engstrom, Ilyas, &

Kwok, 2018) and Auto-PGD(APGD) (Croce & Hein, 2020), and black-box attack includes Bandits (Ilyas et al., 2019). Unless specified otherwise, we set the l_∞ -norm bounded perturbation size to 8/255 and the attack iterations to 20. We report clean accuracy (accuracy on benign data) and robustness (accuracy on adversarial examples).

4.1.2 Robustness under White-box Attacks

Comparison with Bayesian Defense.

Following the evaluation protocol in recent Bayesian defense work (Doan et al., 2022; X. Liu et al., 2019), we combine Expectation-over-Transformation (Athalye, Engstrom, et al., 2018) with PGD attack (Madry et al., 2018) to develop a strong white-box l_∞ -EoT PGD. We set the perturbation budget to $\epsilon \in [0 : 0.07 : 0.005]$ and report the results for BBC, PGD-AT (Madry et al., 2018) and other Bayesian defense in Tab. 2.

Overall, BBC demonstrates superior robustness compared to other defenses, particularly as the attack strength increases. Notably, even at the extreme perturbation of 0.07, BBC still retains 48.4% robustness on CIFAR-10, outperforming the previous state-of-the-art method by 31.9%. More importantly, the robustness improvements are ‘for free’, meaning that BBC does not compromise accuracy and require retraining the model under the black-box defense setting.

Table 2 Comparing robustness(%) under different EoT-PGD attack budget

Data	Defenses	0	0.035	0.055	0.07
CIFAR-10					
	None	93.6	0	0	0
	PGD-AT	80.3	31.1	15.5	10.3
VGG-16	Adv-BNN	79.7	37.7	16.3	8.1
	IG-BNN	83.6	50.2	26.8	16.9
	BBC(Ours)	93.3	79.1	63.1	48.4
STL-10					
	None	78.5	0	0	0
	PGD-AT	63.2	27.4	12.8	7.0
ModelA	Adv-BNN	59.9	31.4	16.7	9.1
	IG-BNN	64.3	48.2	34.9	27.3
	BBC(Ours)	78.2	43.3	41.2	39.3

Comparisons with AT Methods.

We select several state-of-the-art AT methods, including the popular PGD-AT (Madry et al., 2018), TRADES (H. Zhang et al., 2019b) and MART (Y. Wang et al., 2020), as well as the recently proposed LAS-AT (Jia et al., 2022) and AWP (Wu et al., 2020). Moreover, we compare our method with FAT (J. Zhang et al., 2020) and LBGAT (Cui et al., 2021), they also can achieve strong robustness while preserving high accuracy on benign data. All AT methods use the WRN34-10 network. We choose the PGD attack (Madry et al., 2018) for evaluation. The results on CIFAR-10 and CIFAR-100 are reported in Tab. 3, where BBC outperforms the state-of-the-art AT by a large margin on both benign and robust performance. In addition, BBC simultaneously keeps similar high accuracy on adversarial samples and clean data, demonstrating the effectiveness of a full Bayesian treatment on normal data, the adversarial samples and the classifier.

Table 3 Comparing robustness(%) on CIFAR-10 and CIFAR-100

Method	CIFAR-10			CIFAR-100		
	Clean	PGD-20	PGD-50	Clean	PGD-20	PGD-50
ST	96.2	0	0	80.4	0	0
PGD-AT	85.2	55.1	54.9	60.9	31.7	31.5
TRADES	85.7	56.1	55.9	58.6	28.7	26.6
MART	84.2	58.6	58.1	60.8	26.4	25.8
LAS-AT	87.7	60.2	59.8	64.9	36.4	36.1
AWP	85.6	58.1	57.9	60.4	33.9	33.7
FAT	88.0	49.9	48.8	-	-	-
LBGAT	88.2	54.7	54.3	60.6	34.8	34.6
BBC(Ours)	94.7	93.9	93.7	74.4	70.4	69.5

Comparisons with State-of-the-art Robustness Model.

It has been observed that the use of data augmentation and a larger model can improve robust generalization remarkably (Gowal et al., 2020). Hence we compare BBC with Gowal et al. (2020), which uses a larger model, 500K additional unlabeled images extracted from 80M-Ti Million Tiny Images (80M TI) dataset (Torralba, Fergus, & Freeman, 2008) and other carefully designed experimental suites to considerably progress the state-of-the-art performance on multiple robustness benchmarks (Croce et al., 2020). We follow

the evaluation protocol designed by Gowal et al. (2020) to use PGD-40 under l_∞ norm-bounded perturbations of size $\epsilon = 8/255$ and l_2 norm-bounded perturbations of size $\epsilon = 128/255$. As shown in Tab. 4, BBC sets a new state-of-the-art on benign and PGD robust evaluation with no extra data, tiny increased model capacity, and no retraining.

Table 4 Comparing of BBC with Gowal et al. (2020)

Data & Models	Norm	Extra data	Clean	Robust
CIFAR-10				
Gowal et al. (2020)(WRN28-10)	l_∞	80M TI	89.5	64.1
Gowal et al. (2020)(WRN70-16)	l_∞	80M TI	91.1	67.2
BBC(WRN28-10)	l_∞	None	94.7	93.7
Gowal et al. (2020)(WRN70-16)	l_2	80M TI	94.7	82.2
BBC(WRN28-10)	l_2	None	94.7	93.1
CIFAR-100				
Gowal et al. (2020)(WRN70-16)	l_∞	80M TI	69.2	39.0
BBC(WRN28-10)	l_∞	None	74.4	69.5

4.1.3 Robustness under Black-box Attack

Under the black-box attack setting, we evaluate BBC along with AAA (S. Chen et al., 2022) and AT Madry et al. (2018) defenses. Given AAA (S. Chen et al., 2022), another empirical black-box defense, is specially designed to prevent score-based query attacks (SQA), we adapt the protocol of AAA to assess defense using the state-of-the-art SQA Bandits (Ilyas et al., 2019), which jointly leverages a time and data-dependent prior as a predictor of the gradient. We assess the defenses using both l_∞ and l_2 threat models, and adopt the default attack settings as described in Ilyas et al. (2019). Since S. Chen et al. (2022) and Ilyas et al. (2019) do not report results for AT and AAA on CIFAR-10 against l_2 -Bandits, so we only evaluate our method against l_2 -Bandits in Tab. 5. In comparison with AT, both AAA and BBC can improve robustness without hurting accuracy. But unlike AAA, whose robustness shows a big gap with accuracy (-16.4%), the gap of BBC is much smaller (-2.6%) across both l_∞ and l_2 threat models. Again, this demonstrates the superior robustness and accuracy of BBC.

Table 5 Robustness(%) under Bandits attack on CIFAR-10(@query=100/2500)

Method	Norm	Clean	Bandits	
			@100	@2500
ST	$l_\infty=8/255$	96.2	69.9	41.0
AT	$l_\infty=8/255$	87.0	83.6	76.3
AAA	$l_\infty=8/255$	94.8	80.9	78.4
BBC(Ours)	$l_\infty=8/255$	94.7	93.7	93.4
ST	l_2	96.2	1.3	0
BBC(Ours)	l_2	94.7	93.8	92.1

4.2 Experiments on S-HAR

4.2.1 Experimental Settings

We briefly introduce the experimental settings here, and the details are in Appendix B.

Datasets and Classifiers.

We choose three widely adopted benchmark datasets in HAR: HDM05 (Müller et al., 2007), NTU60 (Shahroudy, Liu, Ng, & Wang, 2016) and NTU120 (J. Liu, Shahroudy, et al., 2020). For base classifiers, we employ four recent classifiers: ST-GCN (Yan, Xiong, & Lin, 2018), CTR-GCN (Y. Chen et al., 2021), SGN (P. Zhang et al., 2020) and MS-G3D (Z. Liu, Zhang, Chen, Wang, & Ouyang, 2020). Since the classifiers do not have the same setting (e.g. data needing subsampling (P. Zhang et al., 2020)), we unify the data format. For NTU60 and NTU120, we subsample the frames to 60. For HDM05, we divide the data into 60-frame samples (H. Wang, He, et al., 2021). Finally, we retrain the classifiers following their original settings.

Attack Setting.

We employ state-of-the-art attackers designed for S-HAR: SMART (l_2 attack) (H. Wang, He, et al., 2021), CIASA (l_∞ attack) (J. Liu, Akhtar, & Mian, 2020) and BASAR (l_2 attack) (Diao et al., 2021), and follow their default settings. Further, we use the untargeted attack, which is the most aggressive setting. Since all attackers are iterative approaches and more iterations lead to more aggressive attacks, we use 1000-iteration SMART (SMART-1000) on all datasets, 1000-iteration CIASA (CIASA-1000) on HDM05 and 100-iteration CIASA (CIASA-100) on NTU

60/120, since CIASA-1000 on NTU 60/120 is prohibitively slow (approximately 1 month on one Nvidia RTX 3090 GPU). We use the same iterations for BASAR as in their paper. Same as the evaluation metric used in image experiments, We report clean accuracy and robustness.

Defense Setting.

To our best knowledge, BBC is the first black-box defense for S-HAR. So there is no method for direct comparison. There is a technical report (Zheng et al., 2020) which is a simple direct application of randomized smoothing (RS) (Cohen et al., 2019). We use it as one baseline. Standard AT (Madry et al., 2018) has recently been briefly attempted on HAR (Tanaka et al., 2021), so we use it as a baseline SMART-AT (Diao et al., 2022) which employs SMART as the attacker. We also employ another two baseline methods TRADES (H. Zhang et al., 2019b) and MART (Y. Wang et al., 2020), which are the state-of-the-art defense methods on images. We employ perturbations budget $\epsilon = 0.005$ for AT methods (Madry et al., 2018; Y. Wang et al., 2020; H. Zhang et al., 2019b) and compare other ϵ settings in Sec. 4.2.2.

Computational Complexity.

We use 20-iteration attack for training SMART-AT, TRADES and MART, since more iterations incur much higher computational overhead than BBC, leading to unfair comparison. We compare the training time of BBC with other defenses on all datasets in Tab. 6 (all experiments are conducted on one RTX 3090 GPU). Since BBC does not need to re-train the target model, it is the least time-consuming among all AT methods (Madry et al., 2018; Y. Wang et al., 2020; H. Zhang et al., 2019b), *e.g.* only requiring 12.5%-70% of the training time of others. Although RS needs less training time than BBC, its overall robustness is low and therefore fails to defend against attacks, as shown in Tab. 7.

4.2.2 Robustness under White-box Attacks

We show the results of all models on all datasets in Tab. 7. First, BBC does not severely compromise clean accuracy across models and data. The BBC accuracy is within a small range (+0.6/-0.9%)

Table 6 Training time(hours) of all defense methods

Models	AT	RS	MART	TRADES	BBC
HDM05					
ST-GCN	10.1	1	7.7	10.2	1.2
CTR-GCN	10.1	1.1	10.2	15.4	1.2
SGN	1.4	0.1	1.4	1.1	0.7
MS-G3D	22	1.5	14	16.6	3.4
NTU 60					
ST-GCN	51.7	5.8	49	66.4	34.2
CTR-GCN	93.4	5.6	85.5	96	73.7
SGN	16.7	2.1	11.9	13.1	10.1
MS-G3D	240	23.9	132	217	72
NTU 120					
ST-GCN	29.4	2.1	28.2	35.8	19.7
CTR-GCN	51.6	2.6	52.5	51.7	23.4
SGN	27.5	5.6	18.2	20.5	4.6
MS-G3D	378.3	46.1	214	322	115.3

from that of the standard training, in contrast to the often noticeable accuracy decreased in other defense methods. Next, BBC has the best robustness in all scenarios (training methods vs. classifiers vs. datasets vs. attackers) and often by big margins, especially under extreme SMART-1000 and CIASA-1000 attacks. Overall, BBC can significantly improve the adversarial robustness and eliminate the accuracy-robustness trade-off.

Comparison with other AT methods.

As shown in Tab. 7, all baseline methods perform worse than BBC, sometimes completely fail, *e.g.* failing to defend against SMART-1000 in large-scale datasets (NTU 60 and NTU 120). After investigating their defenses against SMART from iteration 20 to 1000 in Fig. 1, we found the key reason is the baseline methods overly rely on the aggressiveness of the adversaries sampled during training. To verify it, we increase the perturbation budget ϵ from 0.005 to 0.05 during training in TRADES, and plot their clean accuracy & robustness vs. ϵ in Fig. 3. Note that BBC does not rely on a specific attacker. We find TRADES is highly sensitive to ϵ values: larger perturbations in adversarial training improve the defense (albeit still less effective than BBC), but harm the standard accuracy (Fig. 3(a)). Further, sampling adversaries with more iterations (*e.g.* 1000 iterations) during AT may also improve the robustness (still worse than BBC Fig. 3(b)) but is prohibitively slow, while BBC requires much smaller computational overhead (see Sec. 4.2.1).

Table 7 Clean accuracy(%) and robustness(%) on HDM05 (top), NTU60 (middle) and NTU120 (bottom)

HDM05	ST-GCN			CTR-GCN			SGN			MS-G3D		
	Clean	SMART	CIASA	Clean	SMART	CIASA	Clean	SMART	CIASA	Clean	SMART	CIASA
Standard	93.2	0	0	94.2	9.9	8.8	94.2	1.9	0.4	93.8	3.0	3.9
SMART-AT	91.9	10.5	8.6	93.0	22.6	18.3	93.3	3.1	2.5	92.8	28.4	21.3
RS	92.7	3.6	2.9	92.1	17.1	18.3	92.8	7.9	1.5	93.0	4.7	5.0
MART	91.1	17.5	15.0	91.5	29.6	20.4	93.8	2.7	1.5	91.5	39.9	18.2
TRADES	91.5	18.8	13.7	92.8	24.3	23.2	92.3	3.4	0.1	90.0	39.8	41.3
BBC(Ours)	93.0	35.8	30.3	93.2	32.7	31.7	94.7	69.3	68.6	93.6	74.7	74.4

NTU60	ST-GCN			CTR-GCN			SGN			MS-G3D		
	Clean	SMART	CIASA	Clean	SMART	CIASA	Clean	SMART	CIASA	Clean	SMART	CIASA
Standard	76.8	0	0.5	82.9	0	0	86.2	0	2.3	89.4	0.3	2.0
SMART-AT	72.8	0	10.6	83.7	0	19.6	83.3	0	10.5	87.8	0	40.4
RS	75.9	0	4.0	82.7	0	6.7	83.0	0	5.9	88.1	0	10.0
MART	71.9	0	14.6	80.3	0	16.3	83.2	0	14.0	85.4	0	42.2
TRADES	71.4	0	18.7	79.6	0	18.5	82.3	0	19.3	85.2	0	43.8
BBC(Ours)	76.5	28.3	22.0	82.8	22.2	30.8	86.1	51.6	56.5	88.8	60.1	58.4

NTU120	ST-GCN			CTR-GCN			SGN			MS-G3D		
	Clean	SMART	CIASA	Clean	SMART	CIASA	Clean	SMART	CIASA	Clean	SMART	CIASA
Standard	68.3	0	0.6	74.6	0	0.3	74.2	0	0.6	84.7	0.4	1.9
SMART-AT	67.3	0	10.2	75.9	0	8.7	71.3	0	3.8	81.9	0.5	29.8
RS	66.8	0	3.0	74.0	0	3.6	71.4	0	1.0	82.2	0.1	1.3
MART	58.4	0.1	11.3	70.5	0.1	13.8	70.1	0.1	9.8	78.9	0.1	33.4
TRADES	61.4	0.2	10.6	72.0	0	13.4	69.4	0	11.3	79.0	0	35.3
BBC(Ours)	68.3	10.6	15.6	74.6	10.7	16.5	73.5	32.0	46.2	84.7	50.5	50.9

4.2.3 Robustness under Black-box Attacks

Black-box attack in S-HAR is either transfer-based (H. Wang, He, et al., 2021) or decision-based (Diao et al., 2021). However, existing transfer-based attacks (SMART and CIASA) are highly sensitive to the chosen surrogate and the target classifier. According to our preliminary experiments (see Appendix A), transfer-based SMART often fails when certain models are chosen as the surrogate, which suggests that transfer-based attack is not a reliable way of evaluating defense in S-HAR. Therefore we do not employ it for evaluation. BASAR is a decision-based approach, which is truly black-box and has proven to be far more aggressive and shrewd (Diao et al., 2021). We employ its evaluation metrics, i.e. the averaged l_2 joint position deviation (l), averaged l_2 joint acceleration deviation (Δa) and averaged bone length violation percentage ($\Delta B/B$), which all highly correlate to the attack imperceptibility.

We randomly select samples following (Diao et al., 2021) for attack. The results are shown in Tab. 8. BBC can often reduce the quality of adversarial samples, which is reflected in l_2 , Δa and $\Delta B/B$. The increase in these metrics means severer jittering/larger deviations from the original motions, which is very visible and raises suspicion. We show one example in Fig. 2 and include the full results in Appendix A.

4.3 Gradient Obfuscation Evaluation

Since BBC averages the prediction across different models, we investigate whether its robustness is due to obfuscated gradients, because obfuscated gradients can be circumvented and are not truly robust (Athalye, Carlini, & Wagner, 2018). One way to verify this is to test BBC on black-box attacks (Athalye, Carlini, & Wagner, 2018; Tramer et al., 2020), which we have demonstrated

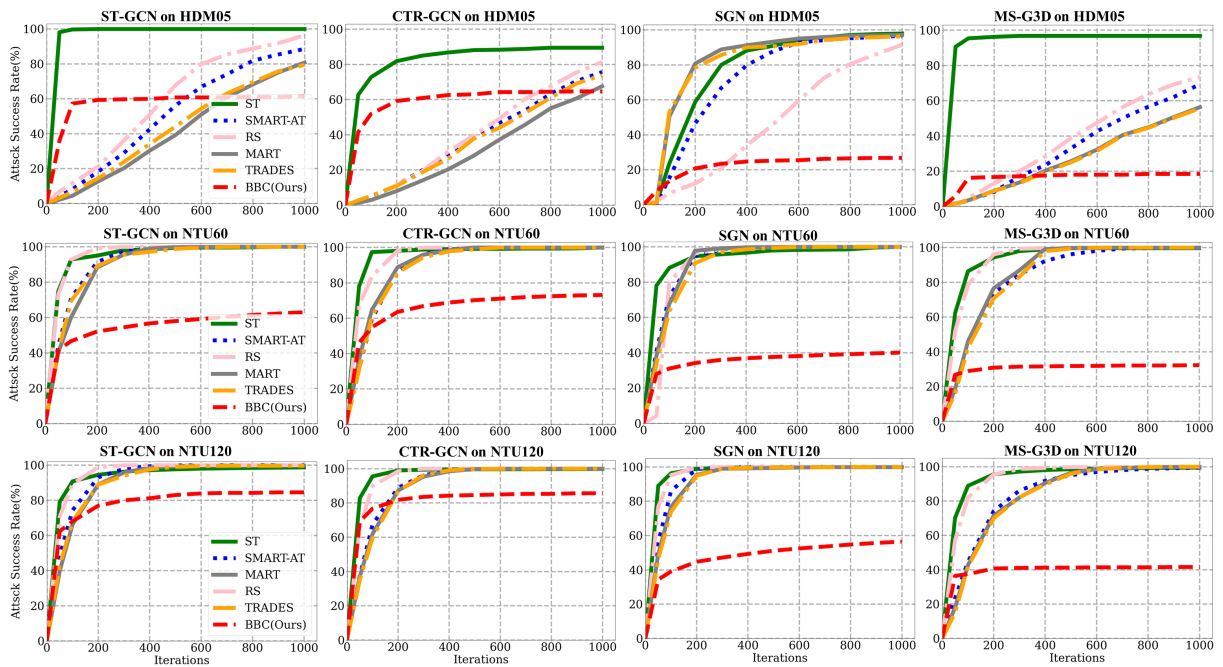


Fig. 1 The attack success rate vs. attack strength curves against SMART. For each subplot, the abscissa axis is iterations while the ordinate axis is the attack success rate(%). ST means standard training

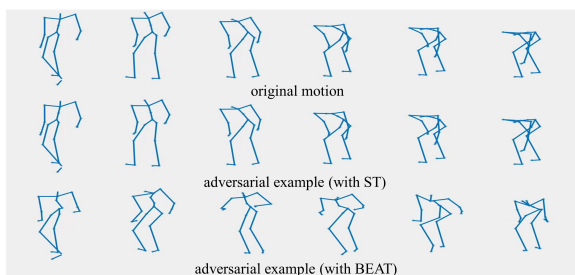


Fig. 2 The original motion ‘deposit’ (top) is attacked by BASAR on standard trained model (middle) and BBC trained model (bottom) separately. The visual difference of the original motion and the attacked motion on BBC is bigger, compared with the attacked motion on ST

in Sec. 4.2.3. To be certain, we utilize Expectation-over-Transformation (EoT) (Athalye, Carlini, & Wagner, 2018) to develop adaptive attacks which can also circumvent defense relying on obfuscated gradients (Tramer et al., 2020). For image classification, we adapt EoT-PGD as mentioned earlier, and the results are reported in Tab. 2. For S-HAR, we deploy an adaptive attack called EoT-SMART based on (Tramer et al., 2020): in each step, we estimate the expected gradient by averaging the gradients of multiple randomly interpolated samples. Tab. 9 shows that EoT-SMART performs

Table 8 Untargeted attack on HDM05 (top), NTU60 (middle) and NTU120 (bottom) from BASAR

	STGCN	CTRGCN	SGN	MSG3D
HDM05				
$l \uparrow$	0.77/ 0.82	0.67/ 0.79	0.84/ 1.05	0.20/ 0.28
$\Delta a \uparrow$	0.21/ 0.22	0.14/0.14	0.05/ 0.07	0.086/ 0.095
$\Delta B/B \uparrow$	0.42%/0.77%	0.80%/0.94%	1.1%/1.5%	1.1%/1.2%
NTU60				
$l \uparrow$	0.03/ 0.05	0.05/ 0.06	0.06/ 0.08	0.09/0.09
$\Delta a \uparrow$	0.015/ 0.017	0.02/ 0.03	0.003/ 0.004	0.03/ 0.04
$\Delta B/B \uparrow$	4.2%/4.8%	6.5%/7.4%	1.3%/1.7%	8.9%/11.0%
NTU120				
$l \uparrow$	0.03/ 0.04	0.04/ 0.06	0.087/ 0.103	0.06/ 0.08
$\Delta a \uparrow$	0.015/ 0.018	0.019/ 0.022	0.005/ 0.006	0.02/ 0.03
$\Delta B/B \uparrow$	4.0%/4.7%	5.4%/5.6%	2.3%/2.7%	6.8%/9.0%

xxx/xxx is pre/post BBC results.

only slightly better than SMART, demonstrating that BBC does not rely on obfuscated gradients.

Table 9 Robustness(%) against EoT-SMART

BBC	ST-GCN	CTR-GCN	SGN	MS-G3D
HDM05	35.1 (-0.7)	29.5 (-3.2)	68.9 (-0.4)	71.8 (-2.9)
NTU 60	28.2 (-0.1)	22.3 (+0.1)	50.0 (-1.6)	58.4 (-0.0)

(\pm xx) means the robustness difference with SMART.

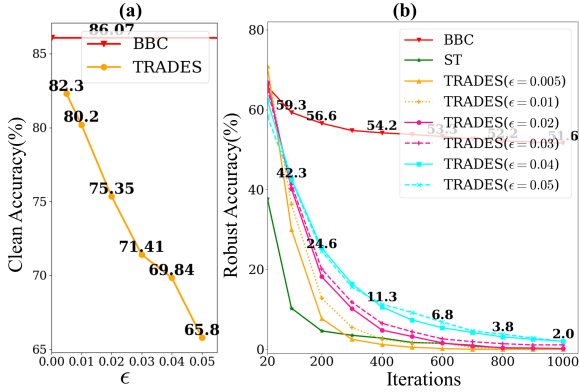


Fig. 3 Comparisons with TRADES with different perturbation budget (ϵ) on NTU60 with SGN. (a): standard accuracy vs. ϵ ; (b): robustness against SMART with 20 to 1000 iterations

4.4 Ablation Study

Number of Appended Models.

Although BNNs theoretically require sampling of many models for inference, in practice, we find a small number of models suffice. To show this, we conduct an ablation study on the number of appended models (N in Eq. (11)). For image classification, we report the robustness against APGD (Croce & Hein, 2020), which is a more competitive adversary than vanilla PGD attack. As shown in Tab. 10, with N increasing, BBC significantly lowers the attack success rates, which shows the Bayesian treatment of the model parameters is able to greatly increase the robustness. Further, when $N > 5$, there is a diminishing gain with a slight improvement in robustness but also with increased computation. This performance is consistent across different models and data types, so we use $N=5$ by default.

Table 10 Robustness(%) under different number of appended models

Num	CIFAR-10(WRN28-10)		NTU60(SGN)	
	Clean	APGD	Clean	SMART
1	92.3	15.9	84.9	3.1
3	93.3	68.9	85.7	36.9
5	94.7	88.7	86.1	51.6
7	94.5	89.2	86.0	62.4

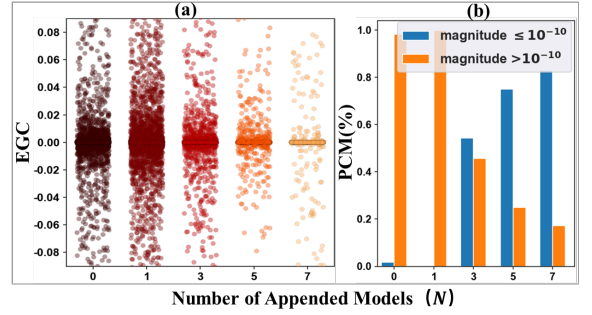


Fig. 4 The components of the expected loss gradients of BBC on NTU60 with SGN. $N = 0$ is standard training. (a): the values of the expected gradient components(EGC); (b): the percentage of the component magnitude (PCM) above and below 10^{-10}

We further show why our *post-train* Bayesian strategy is able to greatly increase the robustness. The classification loss gradient with respect to data is key to many attack methods. In a deterministic model, this gradient is computed on one model; in BBC, this gradient is averaged over all models, i.e. the expected loss gradient. Theoretically, with an infinitely wide network in the large data limit, the expected loss gradient achieves 0, which is the source of the good robustness of BNNs (Bortolussi et al., 2022). To investigate whether BBC’s robustness benefits from the vanishing expected gradient, we randomly sample 500 motions from NTU60 and sample one frame from each motion. Then we compute their expected loss gradients and plot a total of 37500 loss gradient components in Fig. 4 (a), where each dot represents a component of the expected loss gradient of one frame. Fig. 4 (b) shows the percentage of the expected gradient components close to 0. Similarly, we sample 500 images from CIFAR-10 and randomly count for 75000 loss gradient components in Fig. 5. Fig. 4 and Fig. 5 essentially show the empirical distribution of the component-wise expected loss gradient. In both cases, when N increases, the gradient components steadily approach zero, indicating a vanishing expected loss gradient which provides robustness (Bortolussi et al., 2022).

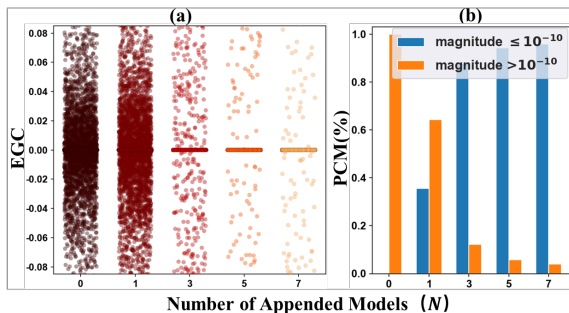


Fig. 5 The components of the expected loss gradients of BBC on CIFAR-10 with WRN28-10

Joint Distribution of Data and Adversaries.

Other than the Bayesian treatment of models, BBC also benefits from the Bayesian treatment on the adversaries. To see its contribution, we plug-and-play our post-train Bayesian strategy to other AT methods which do not model the adversarial distribution. Specially, we keep the pre-trained classifiers intact and then take a post-train Bayesian treatment on TRADES(PB+TRADES). We compare it with BBC. As shown in Tab. 11, PB+TRADES only improves the robustness slightly on image data. On NTU60 with SGN as the base action classifier, PB+TRADES achieves 84.7% clean accuracy and 34.7% robustness against SMART. BBC still outperforms PB+TRADES by large margins, further improving accuracy by 1.3% and robustness by 16.9%. Note the major difference between BBC and PB+TRADES is whether to consider the full adversarial distribution, which shows the benefit of bringing the full adversarial distribution into the joint probability.

Table 11 Ablation Study on CIFAR-10 with VGG-16 as the base classifier

Methods	Clean	PGD	APGD	EoT-PGD
PB+TRADES	93.6	10.7	8.5	3.9
BBC(l_2 distance)	93.4	51.7	32.7	43.4
BBC(perception distance)	93.3	92.5	89.1	81.8

Manifold Representation.

One key novelty of our proposed method is we can dictate the data manifold geometry by parameterizing a distance function $d(\mathbf{x}, \tilde{\mathbf{x}})$. But actually $d(\mathbf{x}, \tilde{\mathbf{x}})$ can also be devised by any other distance-based function to measure the distance between the clean sample and their adversaries. Here we report the performance when l_2 distance, a common distance in AT and RS, is used within our proposed defense framework in Tab. 11. BBC with manifold representation clearly surpasses BBC with l_2 distance-based metric. This is because adversarial samples are typically near the data manifold, both on-manifold and off-manifold (Diao et al., 2021; Stutz et al., 2019). Therefore, devising data/task specific data manifold can better capture the fine-grained structure of the adversarial distribution than simply using Euclidean distance.

Other Settings for Post-train Bayesian Strategy.

Post-train BBC keeps the pre-trained classifier intact and appends a tiny model with parameters θ' behind the classifier using a skip connection: $\text{logits} = f_{\theta'}(\phi(\mathbf{x})) + g_{\theta}(\mathbf{x})$, in contrast to the original $\text{logits} = g_{\theta}(\mathbf{x})$. $\phi(\mathbf{x})$ can be the latent features of \mathbf{x} or the original logits $\phi(\mathbf{x}) = g_{\theta}(\mathbf{x})$. We conduct an ablation study on CIFAR-10 and HDM05 to demonstrate the effectiveness of the both settings. Shown in Tab. 12, the later setting has better benign and defense performance. Moreover, the model choice has implications. When $\phi(\mathbf{x}) = g_{\theta}(\mathbf{x})$ is employed, it enables treating g as a black-box classifier, requiring little prior knowledge about the classifier itself. Arguably, this is a better setting, where the people doing BBC can largely ignore the classifier details as they might not be the people who developed the classifier. So we employ $\phi(\mathbf{x}) = g_{\theta}(\mathbf{x})$ to keep the black-boxness of BBC.

5 Limitation and Discussion

One limitation is prior knowledge is needed on $d(\mathbf{x}, \tilde{\mathbf{x}})$ in Eq. (4), either explicitly as BBC or implicitly e.g. using another model to learn the data manifold. However, this is lightweight as manifold learning/representation is a rather active field and many methods could be used. BBC can

Table 12 Comparison with various $\phi(\mathbf{x})$ settings on CIFAR-10 with VGG-16(top) and on HDM05 with STGCN(bottom)

$\phi(\mathbf{x})$	Clean	APGD	EoT-PGD
Latent Features of \mathbf{x}	92.1	80.9	74.7
Original Logits $g_\theta(\mathbf{x})$	93.4	89.1	81.8

$\phi(\mathbf{x})$	Clean	SMART	CIASA
Latent Features of \mathbf{x}	92.8	35.6	32.8
Original Logits $g_\theta(\mathbf{x})$	93.0	35.8	34.9

potentially incorporate any manifold representation. Also, we assume that all adversarial samples are distributed closely to the data manifold, which is true for images (Stutz et al., 2019) and skeletal motion (Diao et al., 2021), but not necessarily for other data. Further, although BBC is effective on a wide range of AA methods, including white-box, black-box, gradient-based, decision-based and sampling-based approaches, it is less effective on certain optimization-based methods such as auto-attack (Croce & Hein, 2020). Auto-attack employs adaptive step sizes, randomized search and enhanced adversarial loss, making it similar to a global optimization scheme in search for adversarial examples, which is powerful at the cost of time consumption. Sampling more adversarial examples in every epoch slightly mitigates this problem but it is overall not as good as AT methods such as TRADES. Using BBC to re-train the whole model could improve the situation but we choose to retain the black-boxness of the classifiers instead. We argue that the benefit of the black-boxness outweighs the limitation as it gains extra robustness without severely sacrificing the clean accuracy at a small cost.

6 Conclusions and Future Work

To our best knowledge, we proposed a new black-box defense framework and it is the first black-box defense for S-HAR. Our method BBC is underpinned by a new Bayesian Energy-based Adversarial Training framework, and is evaluated across various classifiers, datasets and attackers. Our method employs a post-train strategy for fast training and a full Bayesian treatment on clean data, their adversarial samples and the classifier,

without adding much extra computational cost. In future, we will extend BBC to more data types, both time-series and static, such as videos and graphs, by employing task/data specific $d(\mathbf{x}, \tilde{\mathbf{x}})$ in Eq. (6).

7 Acknowledgment

This project has received funding from the European Union’s Horizon 2020 research and innovation programme under grant agreement No 899739 CrowdDNA.

References

- Athalye, A., Carlini, N., Wagner, D. (2018). Obfuscated gradients give a false sense of security: Circumventing defenses to adversarial examples. *International conference on machine learning* (pp. 274–283).
- Athalye, A., Engstrom, L., Ilyas, A., Kwok, K. (2018). Synthesizing robust adversarial examples. *International conference on machine learning* (pp. 284–293).
- Bai, T., Luo, J., Zhao, J., Wen, B., Wang, Q. (2021). Recent advances in adversarial training for adversarial robustness. *Proceedings of the thirtieth international joint conference on artificial intelligence, IJCAI* (pp. 4312–4321).
- Blei, D.M., Kucukelbir, A., McAuliffe, J.D. (2017). Variational inference: A review for statisticians. *Journal of the American statistical Association*, 112(518), 859–877.
- Bortolussi, L., Carbone, G., Laurenti, L., Patane, A., Sanguinetti, G., Wicker, M. (2022). On the robustness of bayesian neural networks to adversarial attacks. *arXiv preprint arXiv:2207.06154*.
- Brendel, W., Rauber, J., Bethge, M. (2018). Decision-based adversarial attacks: Reliable attacks against black-box machine learning models. *6th international conference on learning representations, ICLR*.

- Carbone, G., Wicker, M., Laurenti, L., Patane, A., Bortolussi, L., Sanguinetti, G. (2020). Robustness of bayesian neural networks to gradient-based attacks. *Advances in Neural Information Processing Systems*, 33, 15602–15613.
- Chakraborty, A., Alam, M., Dey, V., Chattopadhyay, A., Mukhopadhyay, D. (2018, September). Adversarial Attacks and Defences: A Survey. *arXiv:1810.00069 [cs, stat]*. (arXiv: 1810.00069)
- Chen, P.-Y., Zhang, H., Sharma, Y., Yi, J., Hsieh, C.-J. (2017). Zoo: Zeroth order optimization based black-box attacks to deep neural networks without training substitute models. *Proceedings of the 10th acm workshop on artificial intelligence and security* (pp. 15–26).
- Chen, S., Huang, Z., Tao, Q., Wu, Y., Xie, C., Huang, X. (2022). Adversarial attack on attackers: Post-process to mitigate black-box score-based query attacks. *Advances in neural information processing systems*.
- Chen, T., Fox, E., Guestrin, C. (2014). Stochastic gradient hamiltonian monte carlo. *International conference on machine learning* (pp. 1683–1691).
- Chen, Y., Zhang, Z., Yuan, C., Li, B., Deng, Y., Hu, W. (2021). Channel-wise topology refinement graph convolution for skeleton-based action recognition. *Proceedings of the ieee/cvf international conference on computer vision* (pp. 13359–13368).
- Coates, A., Ng, A., Lee, H. (2011). An analysis of single-layer networks in unsupervised feature learning. *Proceedings of the fourteenth international conference on artificial intelligence and statistics* (pp. 215–223).
- Cohen, J., Rosenfeld, E., Kolter, Z. (2019). Certified adversarial robustness via randomized smoothing. *international conference on machine learning* (pp. 1310–1320).
- Croce, F., Andriushchenko, M., Sehwag, V., Debenedetti, E., Flammarion, N., Chiang, M., ... Hein, M. (2020). Robustbench: a standardized adversarial robustness benchmark. *arXiv preprint arXiv:2010.09670*.
- Croce, F., & Hein, M. (2020). Reliable evaluation of adversarial robustness with an ensemble of diverse parameter-free attacks. *International conference on machine learning* (pp. 2206–2216).
- Cui, J., Liu, S., Wang, L., Jia, J. (2021). Learnable boundary guided adversarial training. *Proceedings of the ieee/cvf international conference on computer vision* (pp. 15721–15730).
- Diao, Y., Shao, T., Yang, Y.-L., Zhou, K., Wang, H. (2021). Basar: black-box attack on skeletal action recognition. *Proceedings of the ieee/cvf conference on computer vision and pattern recognition* (pp. 7597–7607).
- Diao, Y., Wang, H., Shao, T., Yang, Y.-L., Zhou, K., Hogg, D. (2022). Understanding the vulnerability of skeleton-based human activity recognition via black-box attack. *arXiv:2211.11312 [cs]*. Retrieved from <https://arxiv.org/abs/2211.11312> (arXiv: 2211.11312)
- Doan, B.G., Abbasnejad, E.M., Shi, J.Q., Ranasinghe, D. (2022). Bayesian learning with information gain provably bounds risk for a robust adversarial defense. *International conference on machine learning* (pp. 5309–5323).
- Dong, Y., Liao, F., Pang, T., Su, H., Zhu, J., Hu, X., Li, J. (2018). Boosting adversarial attacks with momentum. *Proceedings of the ieee conference on computer vision and pattern recognition* (pp. 9185–9193).
- Du, Y., & Mordatch, I. (2020, June). Implicit Generation and Generalization in Energy-Based Models. *arXiv:1903.08689 [cs, stat]*. Retrieved 2021-09-06, from <http://arxiv.org/abs/1903.08689> (arXiv: 1903.08689)

- Goodfellow, I.J., Shlens, J., Szegedy, C. (2015). Explaining and harnessing adversarial examples. Y. Bengio & Y. LeCun (Eds.), *3rd international conference on learning representations, ICLR 2015, san diego, ca, usa, may 7-9, 2015, conference track proceedings*.
- Gowal, S., Qin, C., Uesato, J., Mann, T., Kohli, P. (2020). Uncovering the limits of adversarial training against norm-bounded adversarial examples. *arXiv preprint arXiv:2010.03593*.
- Grathwohl, W., Wang, K.-C., Jacobsen, J.-H., Duvenaud, D., Norouzi, M., Swersky, K. (2020). Your classifier is secretly an energy based model and you should treat it like one. *International Conference on Learning Representations*.
- Hill, M., Mitchell, J.C., Zhu, S. (2021). Stochastic security: Adversarial defense using long-run dynamics of energy-based models. *9th international conference on learning representations, ICLR 2021*.
- Ilyas, A., Engstrom, L., Madry, A. (2019). Prior convictions: Black-box adversarial attacks with bandits and priors. *International conference on learning representations*.
- Jia, X., Zhang, Y., Wu, B., Ma, K., Wang, J., Cao, X. (2022). Las-at: adversarial training with learnable attack strategy. *Proceedings of the ieee/cvf conference on computer vision and pattern recognition* (pp. 13398–13408).
- Karim, F., Majumdar, S., Darabi, H. (2020). Adversarial attacks on time series. *IEEE transactions on pattern analysis and machine intelligence*, 43(10), 3309–3320.
- Kinfu, K.A., & Vidal, R. (2022). Analysis and extensions of adversarial training for video classification. *Proceedings of the ieee/cvf conference on computer vision and pattern recognition* (pp. 3416–3425).
- Krizhevsky, A., Hinton, G., et al. (2009). Learning multiple layers of features from tiny images.
- Kurakin, A., Goodfellow, I., Bengio, S. (2016). Adversarial examples in the physical world. *arXiv preprint arXiv:1607.02533*.
- Laidlaw, C., Singla, S., Feizi, S. (2021). Perceptual adversarial robustness: Defense against unseen threat models. *International conference on learning representations*.
- Lecuyer, M., Atlidakis, V., Geambasu, R., Hsu, D., Jana, S. (2019). Certified robustness to adversarial examples with differential privacy. *2019 ieee symposium on security and privacy (sp)* (pp. 656–672).
- Lee, K., Yang, H., Oh, S.-Y. (2020). Adversarial training on joint energy based model for robust classification and out-of-distribution detection. *2020 20th International Conference on Control, Automation and Systems (ICCAS)*, 17-21.
- Liu, C., Salzmann, M., Lin, T., Tomioka, R., Süsstrunk, S. (2020). On the Loss Landscape of Adversarial Training: Identifying Challenges and How to Overcome Them. *Advances in Neural Information Processing Systems* (Vol. 33, pp. 21476–21487).
- Liu, J., Akhtar, N., Mian, A. (2020, December). Adversarial Attack on Skeleton-Based Human Action Recognition. *IEEE transactions on neural networks and learning systems, PP*.
- 10.1109/TNNLS.2020.3043002
- Liu, J., Shahroudy, A., Perez, M., Wang, G., Duan, L.-Y., Kot, A.C. (2020). NTU RGB+D 120: A large-scale benchmark for 3D human activity understanding. *IEEE Transactions on Pattern Analysis and Machine Intelligence*, 42(10), 2684–2701.

- Liu, Q., & Wang, D. (2016). Stein variational gradient descent: A general purpose bayesian inference algorithm. *Advances in neural information processing systems*, 29.
- Liu, X., Li, Y., Wu, C., Hsieh, C. (2019). Adv-bnn: Improved adversarial defense through robust bayesian neural network. *International conference on learning representations*.
- Liu, Z., Zhang, H., Chen, Z., Wang, Z., Ouyang, W. (2020). Disentangling and Unifying Graph Convolutions for Skeleton-Based Action Recognition. *Proceedings of the IEEE/CVF Conference on Computer Vision and Pattern Recognition* (pp. 143–152).
- Madry, A., Makelov, A., Schmidt, L., Tsipras, D., Vladu, A. (2018). Towards Deep Learning Models Resistant to Adversarial Attacks. *International Conference on Learning Representations*. Retrieved from <https://openreview.net/forum?id=rJzIBfZAb>
- Mustafa, A., Khan, S.H., Hayat, M., Goecke, R., Shen, J., Shao, L. (2020). Deeply supervised discriminative learning for adversarial defense. *IEEE transactions on pattern analysis and machine intelligence*, 43(9), 3154–3166.
- Müller, M., Röder, T., Clausen, M., Eberhardt, B., Krüger, B., Weber, A. (2007, June). *Documentation Mocap Database HDM05* (Tech. Rep. No. CG-2007-2). Universität Bonn. (ISSN: 1610-8892)
- Neal, R.M. (2012). *Bayesian learning for neural networks* (Vol. 118). Springer Science & Business Media.
- Nie, W., Guo, B., Huang, Y., Xiao, C., Vahdat, A., Anandkumar, A. (2022). Diffusion models for adversarial purification. *International conference on machine learning* (pp. 16805–16827).
- Nijkamp, E., Hill, M., Han, T., Zhu, S.-C., Wu, Y.N. (2019, November). On the Anatomy of MCMC-Based Maximum Likelihood Learning of Energy-Based Models. *arXiv:1903.12370 [cs, stat]*. Retrieved 2021-09-06, from <http://arxiv.org/abs/1903.12370> (arXiv: 1903.12370)
- Pony, R., Naeh, I., Mannor, S. (2021). Over-the-air adversarial flickering attacks against video recognition networks. *Proceedings of the IEEE/CVF conference on computer vision and pattern recognition* (pp. 515–524).
- Qin, C., Martens, J., Goyal, S., Krishnan, D., Dvijotham, K., Fawzi, A., ... Kohli, P. (2019). Adversarial robustness through local linearization. *Advances in Neural Information Processing Systems*, 32.
- Rade, R., & Moosavi-Dezfooli, S.-M. (2022). Reducing excessive margin to achieve a better accuracy vs. robustness trade-off. *International conference on learning representations*.
- Raghuathan, A., Xie, S.M., Yang, F., Duchi, J., Liang, P. (2020). Understanding and mitigating the tradeoff between robustness and accuracy. *International conference on machine learning* (pp. 7909–7919).
- Rice, L., Wong, E., Kolter, J.Z. (2020). Overfitting in adversarially robust deep learning. *Proceedings of the 37th international conference on machine learning, ICML 2020, 13-18 july 2020, virtual event* (Vol. 119, pp. 8093–8104). PMLR.
- Saatci, Y., & Wilson, A.G. (2017). Bayesian gan. *Advances in neural information processing systems* (Vol. 30).
- Shahroudy, A., Liu, J., Ng, T.-T., Wang, G. (2016). NTU RGB+D: A large scale dataset for 3D human activity analysis. *Proceedings of the IEEE conference on computer vision and pattern recognition* (pp. 1010–1019).
- Springenberg, J.T., Klein, A., Falkner, S., Hutter, F. (2016). Bayesian optimization with

- robust bayesian neural networks. (Vol. 29).
- Stutz, D., Hein, M., Schiele, B. (2019). Disentangling adversarial robustness and generalization. *Cvpr* (pp. 6976–6987).
- Tanaka, N., Kera, H., Kawamoto, K. (2021). Adversarial bone length attack on action recognition. *arXiv preprint arXiv:2109.05830*.
- Tang, X., Wang, H., Hu, B., Gong, X., Yi, R., Kou, Q., Jin, X. (2022, jul). Real-time controllable motion transition for characters. *ACM Trans. Graph.*, 41(4). Retrieved from <https://doi.org/10.1145/3528223.3530090>
- 10.1145/3528223.3530090
- Tieleman, T. (2008, July). Training restricted Boltzmann machines using approximations to the likelihood gradient. *Proceedings of the 25th international conference on Machine learning* (pp. 1064–1071). New York, NY, USA: Association for Computing Machinery. Retrieved 2021-09-06, from <https://doi.org/10.1145/1390156.1390290>
- 10.1145/1390156.1390290
- Torrallba, A., Fergus, R., Freeman, W.T. (2008). 80 million tiny images: A large data set for nonparametric object and scene recognition. *IEEE transactions on pattern analysis and machine intelligence*, 30(11), 1958–1970.
- Tramer, F., Carlini, N., Brendel, W., Madry, A. (2020). On adaptive attacks to adversarial example defenses. *Advances in Neural Information Processing Systems*, 33, 1633–1645.
- Tsipras, D., Santurkar, S., Engstrom, L., Turner, A., Madry, A. (2019). Robustness may be at odds with accuracy. *International conference on learning representations*.
- Wang, H., Diao, Y., Tan, Z., Guo, G. (2023, June). Defending black-box skeleton-based human activity classifiers. *Proceedings of the aaai conference on artificial intelligence*.
- Wang, H., He, F., Peng, Z., Shao, T., Yang, Y., Zhou, K., Hogg, D. (2021, June). Understanding the Robustness of Skeleton-based Action Recognition under Adversarial Attack. *Proceedings of the IEEE/CVF Conference on Computer Vision and Pattern Recognition (CVPR)*.
- Wang, H., Ho, E.S., Komura, T. (2015). An energy-driven motion planning method for two distant postures. *IEEE transactions on visualization and computer graphics*, 21(1), 18–30. (Publisher: IEEE)
- Wang, H., Ho, E.S.L., Shum, H.P.H., Zhu, Z. (2021). Spatio-Temporal Manifold Learning for Human Motions via Long-Horizon Modeling. *IEEE Transactions on Visualization and Computer Graphics*, 27(1), 216–227.
- 10.1109/TVCG.2019.2936810
- Wang, H., Sidorov, K.A., Sandilands, P., Komura, T. (2013). Harmonic parameterization by electrostatics. *ACM Transactions on Graphics (TOG)*, 32(5), 155.
- Wang, Y., Zou, D., Yi, J., Bailey, J., Ma, X., Gu, Q. (2020). Improving adversarial robustness requires revisiting misclassified examples. *International conference on learning representations*.
- Wei, X., Zhu, J., Yuan, S., Su, H. (2019). Sparse adversarial perturbations for videos. *Proceedings of the aaai conference on artificial intelligence* (Vol. 33, pp. 8973–8980).
- Wei, Z., Chen, J., Wei, X., Jiang, L., Chua, T., Zhou, F., Jiang, Y. (2020). Heuristic black-box adversarial attacks on video recognition models. *The thirty-fourth AAAI conference on artificial intelligence* (pp. 12338–12345).
- Welling, M., & Teh, Y.W. (2011, June). Bayesian learning via stochastic gradient langevin dynamics. *Proceedings of the 28th International Conference on International Conference on Machine Learning* (pp. 681–688). Madison, WI, USA: Omnipress.

- Wu, D., Xia, S.-T., Wang, Y. (2020). Adversarial weight perturbation helps robust generalization. *Advances in Neural Information Processing Systems*, 33, 2958–2969.
- Xu, X., Li, L., Li, B. (2022). Lot: Layer-wise orthogonal training on improving l2 certified robustness. *Advances in neural information processing systems*.
- Yan, S., Xiong, Y., Lin, D. (2018). Spatial temporal graph convolutional networks for skeleton-based action recognition. *Thirty-second AAAI conference on artificial intelligence*.
- Yang, Y., Rashtchian, C., Zhang, H., Salakhutdinov, R.R., Chaudhuri, K. (2020). A closer look at accuracy vs. robustness. *Advances in neural information processing systems*.
- Ye, N., & Zhu, Z. (2018). Bayesian adversarial learning. (Vol. 31).
- Zagoruyko, S., & Komodakis, N. (2016). Wide residual networks. *British machine vision conference 2016*.
- Zhang, D., Ye, M., Gong, C., Zhu, Z., Liu, Q. (2020). Black-box certification with randomized smoothing: A functional optimization based framework. *Advances in neural information processing systems* (Vol. 33, pp. 2316–2326).
- Zhang, H., Yu, Y., Jiao, J., Xing, E., El Ghaoui, L., Jordan, M. (2019a). Theoretically principled trade-off between robustness and accuracy. *International conference on machine learning* (pp. 7472–7482).
- Zhang, H., Yu, Y., Jiao, J., Xing, E., El Ghaoui, L., Jordan, M. (2019b). Theoretically principled trade-off between robustness and accuracy. *International conference on machine learning* (pp. 7472–7482).
- Zhang, J., Xu, X., Han, B., Niu, G., Cui, L., Sugiyama, M., Kankanhalli, M. (2020). Attacks which do not kill training make adversarial learning stronger. *International conference on machine learning* (pp. 11278–11287).
- Zhang, P., Lan, C., Zeng, W., Xing, J., Xue, J., Zheng, N. (2020). Semantics-Guided Neural Networks for Efficient Skeleton-Based Human Action Recognition. *Proceedings of the IEEE Conference on Computer Vision and Pattern Recognition*.
- Zhang, R., Isola, P., Efros, A.A., Shechtman, E., Wang, O. (2018). The unreasonable effectiveness of deep features as a perceptual metric. *Proceedings of the IEEE conference on computer vision and pattern recognition* (pp. 586–595).
- Zhang, Y., Yao, Y., Jia, J., Yi, J., Hong, M., Chang, S., Liu, S. (2022). How to robustify black-box ml models? a zeroth-order optimization perspective. *International conference on learning representations*.
- Zhang, Z., Li, W., Bao, R., Harimoto, K., Wu, Y., Sun, X. (2023). Asat: Adaptively scaled adversarial training in time series. *Neurocomputing*, 522, 11–23.
- Zheng, T., Liu, S., Chen, C., Yuan, J., Li, B., Ren, K. (2020). Towards understanding the adversarial vulnerability of skeleton-based action recognition. *arXiv preprint arXiv:2005.07151*.
- Zhu, Y., Ma, J., Sun, J., Chen, Z., Jiang, R., Chen, Y., Li, Z. (2021). Towards understanding the generative capability of adversarially robust classifiers. *Proceedings of the IEEE/CVF international conference on computer vision* (pp. 7728–7737).

A Further Results on S-HAR

Here we first report the defense evaluation under transfer-based SMART attack. As shown in Appendix A, when using 2S-AGCN (?) as the surrogate model, the attack success rate is low on three of the four targeted models. This confirms the sensitivity of SMART on the chosen surrogate during transfer-based attack (H. Wang, He, et al., 2021) and suggests that transfer-based attack is not a reliable way of evaluating defense. Therefore, we do not employ it to test the robustness of BBC.

Table 13 Defense against transfer-based SMART

NTU 60		ST-GCN	CTR-GCN	SGN	MSG3D
SMART	ST	1.56%	0.94%	74.10%	0.2%
	BBC	0.60%	0.63%	70.12%	0.2%

‘SMART’ is the attack success rate of transfer-based SMART, using 2S-AGCN as the surrogate model. ‘ST’ means standard training. The attack success rate for transfer-based SMART is low on ST-GCN, CTR-GCN and MSG3D in both ST and BBC.

To test defense against black-box attack, we employ BASAR (Diao et al., 2021). As BASAR can always achieve 100% attack success, we need to evaluate the quality of the adversarial samples. The lower the quality is, the more effective our defense is. We employ several metrics to measure the attack quality, following (Diao et al., 2021). They are the l_2 joint position deviation (l), l_2 joint acceleration deviation (Δa), l_2 joint angular acceleration deviation ($\Delta \alpha$), bone length violation percentage ($\Delta B/B$) and on-manifold sample percentage (OM). To comprehensively evaluate the defense performance, we show the maximum and mean value of these metrics, and the percentage of $l \geq a_1$ and $\Delta B/B \geq a_2$, where a_1 and a_2 are the thresholds. The mean metric gives the general quality of the attack, the max shows the worst quality of the attack and the percentage shows how many adversarial samples are above pre-defined thresholds on different metrics. The thresholds are chosen empirically based on classifiers and datasets, as the visual quality of adversarial samples vary. We chose the thresholds beyond which the visual difference between adversarial samples and the original motions become noticeable.

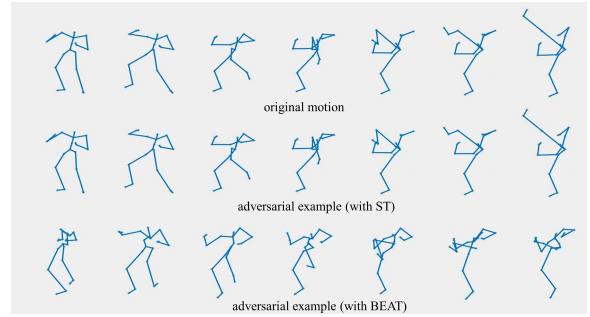


Fig. 6 The original motion ‘kick’ (top) is attacked by BASAR on standard trained model (middle) and BBC trained model (bottom) separately. The adversarial sample under BBC becomes visually different from the original motion.

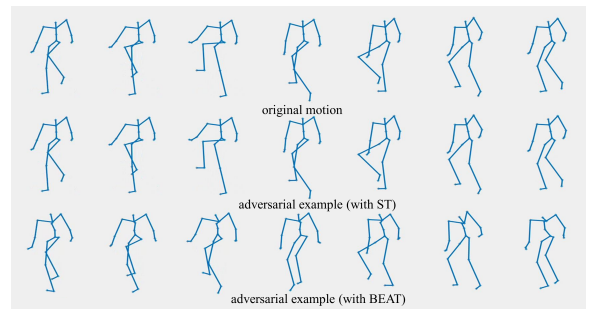


Fig. 7 The original motion ‘climb’ (top) is attacked by BASAR on standard trained model (middle) and BBC trained model (bottom) separately. The adversarial sample under BBC becomes visually different from the original motion.

The results are shown in Tab. 14-17. First, BBC can often reduce the quality of adversarial samples as shown in mean, max and thresholded metrics. This is reflected in l_2 , Δa , $\Delta \alpha$ and $\Delta B/B$. The increase in these metrics normally means there is severe jittering starting to appear in the adversarial samples, which is very visible and can raise suspicion. These attacks tend to fail in that humans would be able to detect them. Further, BBC can often make adversarial samples more perceptible as OM decreases. It means more adversarial samples deviate from the normal data manifold, suggesting an overall lower quality of the adversarial samples, after BBC training. Here we provide more visual results in Fig. 6 and Fig. 7.

B Experimental Settings

We used one Nvidia RTX 3090 GPU for all experiments. All implementation is on Pytorch. In

Table 14 Defense against BASAR on STGCN

STGCN HDM05	Accuracy	Threshold		Max				Mean				
		$l \geq 3 \uparrow$	$\Delta B/B \geq 5\% \uparrow$	$l \uparrow$	$\Delta a \uparrow$	$\Delta \alpha \uparrow$	$\Delta B/B \uparrow$	$l \uparrow$	$\Delta a \uparrow$	$\Delta \alpha \uparrow$	$\Delta B/B \uparrow$	OM \downarrow
ST	92.66%	3.6%	2.3%	4.2	0.96	1.52	4.2%	0.77	0.21	0.41	0.42%	90.55%
BBC(Ours)	92.46%	6.4%	5.4%	5.6	1.32	2.91	5.3%	0.82	0.22	0.46	0.77%	78.36%
NTU60	Accuracy	$l \geq 0.1 \uparrow$	$\Delta B/B \geq 10\% \uparrow$	$l \uparrow$	$\Delta a \uparrow$	$\Delta \alpha \uparrow$	$\Delta B/B \uparrow$	$l \uparrow$	$\Delta a \uparrow$	$\Delta \alpha \uparrow$	$\Delta B/B \uparrow$	OM \downarrow
ST	76.81%	3.7%	8.8%	0.22	0.08	0.13	19.4%	0.03	0.015	0.023	4.2%	0%
BBC(Ours)	74.47%	8.1%	14.4%	0.98	0.11	0.16	43.0%	0.05	0.017	0.024	4.8%	0%
NTU120	Accuracy	$l \geq 0.1 \uparrow$	$\Delta B/B \geq 10\% \uparrow$	$l \uparrow$	$\Delta a \uparrow$	$\Delta \alpha \uparrow$	$\Delta B/B \uparrow$	$l \uparrow$	$\Delta a \uparrow$	$\Delta \alpha \uparrow$	$\Delta B/B \uparrow$	OM \downarrow
ST	68.34%	5.1%	5.1%	0.19	0.08	0.17	29.3%	0.03	0.015	0.016	4.0%	3.8%
BBC(Ours)	66.84%	7.6%	8.7%	0.32	0.14	0.26	37.4%	0.04	0.018	0.02	4.7%	3.3%

ST means standard training. Metrics are computed on the adversarial samples computed after ST training and BBC training.

Table 15 Defense against BASAR on CTRGCN

CTRGCN HDM05	Accuracy	Threshold		Max				Mean				
		$l \geq 3 \uparrow$	$\Delta B/B \geq 5\% \uparrow$	$l \uparrow$	$\Delta a \uparrow$	$\Delta \alpha \uparrow$	$\Delta B/B \uparrow$	$l \uparrow$	$\Delta a \uparrow$	$\Delta \alpha \uparrow$	$\Delta B/B \uparrow$	OM \downarrow
ST	95.10%	5.0%	1.7%	6.7	0.28	1.78	8.5%	0.67	0.14	0.31	0.80%	45.0%
BBC(Ours)	94.73%	9.9%	3.2%	6.0	0.37	3.39	7.0%	0.79	0.14	0.38	0.94%	44.4%
NTU60	Accuracy	$l \geq 0.1 \uparrow$	$\Delta B/B \geq 10\% \uparrow$	$l \uparrow$	$\Delta a \uparrow$	$\Delta \alpha \uparrow$	$\Delta B/B \uparrow$	$l \uparrow$	$\Delta a \uparrow$	$\Delta \alpha \uparrow$	$\Delta B/B \uparrow$	OM \downarrow
ST	82.90%	14.0%	19.4%	0.53	0.12	0.31	37.9%	0.05	0.02	0.03	6.5%	2.2%
BBC(Ours)	82.24%	18.9%	22.6%	0.57	0.12	0.45	52.8%	0.06	0.03	0.04	7.4%	0.9%
NTU120	Accuracy	$l \geq 0.1 \uparrow$	$\Delta B/B \geq 10\% \uparrow$	$l \uparrow$	$\Delta a \uparrow$	$\Delta \alpha \uparrow$	$\Delta B/B \uparrow$	$l \uparrow$	$\Delta a \uparrow$	$\Delta \alpha \uparrow$	$\Delta B/B \uparrow$	OM \downarrow
ST	74.59%	14.0%	14.8%	0.53	0.13	0.2	34.0%	0.04	0.019	0.02	5.4%	1.7%
BBC(Ours)	74.25%	18.0%	16.8%	1.54	0.28	0.2	47.0%	0.06	0.022	0.02	5.6%	1.0%

Table 16 Defense against BASAR on SGN

SGN HDM05	Accuracy	Threshold		Max				Mean				
		$l \geq 5 \uparrow$	$\Delta B/B \geq 10\% \uparrow$	$l \uparrow$	$\Delta a \uparrow$	$\Delta \alpha \uparrow$	$\Delta B/B \uparrow$	$l \uparrow$	$\Delta a \uparrow$	$\Delta \alpha \uparrow$	$\Delta B/B \uparrow$	OM \downarrow
ST	94.16%	5.6%	5.1%	20.5	1.2	10.8	22.3%	0.84	0.05	0.38	1.1%	88.8%
BBC(Ours)	93.78%	8.8%	7.7%	15.5	1.6	10.7	24.5%	1.05	0.07	0.56	1.5%	87.9%
NTU60	Accuracy	$l \geq 0.1 \uparrow$	$\Delta B/B \geq 10\% \uparrow$	$l \uparrow$	$\Delta a \uparrow$	$\Delta \alpha \uparrow$	$\Delta B/B \uparrow$	$l \uparrow$	$\Delta a \uparrow$	$\Delta \alpha \uparrow$	$\Delta B/B \uparrow$	OM \downarrow
ST	86.22%	13.7%	6.8%	0.76	0.04	0.13	18.5%	0.06	0.003	0.01	1.3%	82.9%
BBC(Ours)	86.00%	16.8%	8.9%	1.02	0.08	0.35	21.5%	0.08	0.004	0.02	1.7%	75.6%
NTU120	Accuracy	$l \geq 0.2 \uparrow$	$\Delta B/B \geq 10\% \uparrow$	$l \uparrow$	$\Delta a \uparrow$	$\Delta \alpha \uparrow$	$\Delta B/B \uparrow$	$l \uparrow$	$\Delta a \uparrow$	$\Delta \alpha \uparrow$	$\Delta B/B \uparrow$	OM \downarrow
ST	74.15%	13.2%	9.9%	1.25	0.01	0.54	40.2%	0.087	0.005	0.022	2.3%	75.4%
BBC(Ours)	73.54%	20.4%	14.0%	0.80	0.05	0.23	37.7%	0.103	0.006	0.023	2.7%	73.1%

this section, we give more details regarding our experimental settings.

B.1 Training Details of BBC

In SGLD in Eq. (16) and Eq. (18), instead of using an identity matrix as the covariance matrix for E_t , we use $\sigma^2 \mathbf{I}$ where $\sigma = 0.005$. In Algorithm 1, we set $M_1 = 10$, $M_2 = 10$ and $b = 0.05$. In Eq. (17), we

use $\lambda = 10^{-3}$. In Eq. (13), τ is automatically chosen (Springenberg et al., 2016). We set $F = 10^{-5}$. We also run Eq. (13) $M_{\theta'} = 30$ steps each time for sampling. One thing to notice is that in Line 13-15 in Algorithm 1, only one \tilde{x} is sampled in each iteration. To model $p_{\theta}(\tilde{\mathbf{x}}|\mathbf{x}, y)$, multiple \tilde{x} can indeed be sampled. In practice, we find one sample in every iteration can give good performances, because in different iterations different \tilde{x} s are sampled.

Table 17 Defense against BASAR on MSG3D

MSG3D HDM05	Accuracy	Threshold		Max				Mean				
		$l \geq 1 \uparrow$	$\Delta B/B \geq 10\% \uparrow$	$l \uparrow$	$\Delta a \uparrow$	$\Delta \alpha \uparrow$	$\Delta B/B \uparrow$	$l \uparrow$	$\Delta a \uparrow$	$\Delta \alpha \uparrow$	$\Delta B/B \uparrow$	OM \downarrow
ST	93.78%	0%	0%	0.51	0.25	0.91	2.97%	0.20	0.086	0.23	1.1%	5.1%
BBC(Ours)	93.97%	3.3%	0%	3.51	0.32	11.53	3.56%	0.28	0.095	0.50	1.2%	4.4%
NTU60	Accuracy	$l \geq 0.1 \uparrow$	$\Delta B/B \geq 15\% \uparrow$	$l \uparrow$	$\Delta a \uparrow$	$\Delta \alpha \uparrow$	$\Delta B/B \uparrow$	$l \uparrow$	$\Delta a \uparrow$	$\Delta \alpha \uparrow$	$\Delta B/B \uparrow$	OM \downarrow
ST	89.36%	24.2%	13.1%	0.57	0.17	0.87	53.8%	0.09	0.03	0.15	8.9%	2.0%
BBC(Ours)	89.16%	31.4%	22.9%	0.39	0.18	0.79	75.2%	0.09	0.04	0.18	11.0%	0%
NTU120	Accuracy	$l \geq 0.1 \uparrow$	$\Delta B/B \geq 15\% \uparrow$	$l \uparrow$	$\Delta a \uparrow$	$\Delta \alpha \uparrow$	$\Delta B/B \uparrow$	$l \uparrow$	$\Delta a \uparrow$	$\Delta \alpha \uparrow$	$\Delta B/B \uparrow$	OM \downarrow
ST	84.71%	14.3%	6.3%	0.29	0.10	0.50	34.3%	0.06	0.02	0.11	6.8%	0%
BBC(Ours)	82.70%	24.6%	23.2%	0.51	0.17	0.71	60.0%	0.08	0.03	0.15	9.0%	0%

In practice, we weight the h_1, h_2, h_3 in Algorithm 1:

$$\mathbf{h}_{g'}/\mathbf{h} = w_1 h_1 + w_2 h_2 + w_3 h_3 \quad (22)$$

The weights in Eq. (22), ϵ in Eq. (16) and Eq. (18), and σ in Eq. (13) can be grouped into several universal settings according to different datasets. Unless specified otherwise, we use $w_1 = 1$, $w_2 = 0.3$, $w_3 = 0.1$, $\epsilon = 0.01$ by default. On HDM05, $\sigma = 0.001$ for STGCN and MSG3D, $\sigma = 0.01$ for CTRGCN and $\sigma = 0.005$ for SGN. On NTU60, $w_1 = 1, w_2 = 0.1, w_3 = 0.05$ and $\sigma = 0.002$ for CTRGCN, and $\sigma = 0.0015$ for MSG3D. On NTU60 and NTU120, $\sigma = 0.005$ for SGN and $w_1 = 1, w_2 = 0.01, w_3 = 0.005$, $\epsilon = 2$ and $\sigma = 0.5$ for STGCN. On NTU120, $\sigma = 0.0015$ for CTRGCN and $\sigma = 10^{-4}$ for MSG3D.

Given that decision-based attack tends to use bigger perturbations, we increase w_3 in Eq. (22) and b in Algorithm 1 when defending against decision-based attack. Unless specified otherwise, we use $w_1 = 1$, $w_2 = 0.1$, $w_3 = 1$, $b = 0.5$, $\sigma = 0.02, M_1 = 2$ and $M_2 = 2$ by default in defense against black-box attack. The decreasing of sampling iterations is to increase the randomness of $\tilde{\mathbf{x}}$. For STGCN on NTU60, we use $b = 1$. For CTRGCN on NTU60 and NTU120, we use $w_1 = 1$, $w_2 = 0.01$, $w_3 = 1$ and $b = 1$. For SGN on NTU120, we set $w_1 = 1$, $w_2 = 0.01$, $w_3 = 10$ and $b = 1$.

B.2 Settings on S-HAR

Unlike there are standard robustness evaluation benchmarks on image data, no similar protocol has been proposed for S-HAR. Hence we give detailed evaluation settings on S-HAR.

Datasets:

We choose three widely adopted benchmark datasets in HAR: HDM05 (Müller et al., 2007), NTU60 (Shahroudy et al., 2016) and NTU120 (J. Liu, Shahroudy, et al., 2020). HDM05 dataset has 130 action classes, 2337 sequences from 5 non-professional actors. NTU60 and NTU120 have two settings: cross-subject and cross-view. We only use the cross-subject data. NTU60 includes 56568 skeleton sequences with 60 action classes, performed by 40 subjects. NTU120 extends NTU60 with an additional 57,367 skeleton sequences over 60 extra action classes, totalling 113,945 samples over 120 classes captured from 106 distinct subjects. We follow the protocols in (Diao et al., 2021; H. Wang, He, et al., 2021) for pre-processing.

Detailed Attack Setting:

Here we report the detailed robustness evaluation. To test the classifier robustness, we employ state-of-the-art attackers designed for skeleton-based HAR: SMART (H. Wang, He, et al., 2021), CIASA (J. Liu, Akhtar, & Mian, 2020) and BASAR (Diao et al., 2021), and follow their default settings. Further, we use the untargeted attack, which is the most aggressive setting. SMART is the l_2 norm-based white-box attack, whose learning rate is set as 0.005. CIASA is the l_∞ norm-based white-box attack, whose learning rate is set as 0.005, and the perturbation budgets define different clipping strengths for different joint. Following their paper, the variables are set to 0.01, 0.05, 0.15, 0.25 for the joint hips, knees, ankles, and feet, respectively. Since all attackers are iterative approaches and more iterations lead to more aggressive attacks, we evaluate the defenders with 1000-iteration SMART attack on

all datasets, CIASA-1000 on HDM05 and CIASA-100 on NTU 60/120 since running CIASA-1000 on NTU 60/120 is prohibitively slow (approximately 1 month on one Nvidia RTX 3090 GPU). BASAR is the l_2 norm-based black-box threat model. We use the same iterations as in their paper, i.e. 500 iterations on HDM05 and 1000 iterations on NTU 60/NTU 120. After training, we collect the correctly classified testing samples for attack.

Random Smoothing setting:

For RS, we follow (Zheng et al., 2020) and the defense strategy is:

$$\arg \max_{y \in \mathbf{y}} p(g_{\theta}(\hat{\mathbf{x}}) = y) \quad (23)$$

where $y \in \mathbf{y}$ is the class label. $\hat{\mathbf{x}}$ is the noisy samples, generated by adding a Gaussian noise to the original sample then temporal-filtering it by a 1×5 Gaussian kernel. The Gaussian noise is drawn from $\mathcal{N}(0, \delta^2 \mathbf{I})$ where δ is the standard deviation, \mathbf{I} is an identity matrix. We set $\delta = 0.5$ on HDM05. Our preliminary experiments show setting $\delta = 0.5$ on NTU 60/120 severely compromise the accuracy, so we set $\delta = 0.1$ on both NTU60 and NTU120.